

UNIVERSITÄTSKLINIKUM HAMBURG-EPPENDORF

Institut der Pathologie mit den Sektionen Molekularpathologie und Zytopathologie

Director: Prof. Dr. med. Guido Sauter

**Upregulation of CD112R (PVRIG) and PD-1 on
cytotoxic T-cells located in T-cell niche of
colorectal cancer**

Dissertation

zur Erlangung des Grades eines Doktors der Medizin
an der Medizinischen Fakultät der Universität Hamburg

vorgelegt von:
Cheng Yang
aus China

Hamburg 2021

(wird von der Medizinischen Fakultät ausgefüllt)

**Angenommen von der
Medizinischen Fakultät der Universität Hamburg am: 17.12.2021**

**Veröffentlicht mit Genehmigung der
Medizinischen Fakultät der Universität Hamburg.**

Prüfungsausschuss, der/die Vorsitzende: PD Dr. Andrea Kristina Horst

Prüfungsausschuss, zweite/r Gutachter/in: Prof. Dr. Guido Sauter

Table of contents

1. Introduction	3
1.1 Historic development of immune checkpoint therapies	3
1.2 Immune checkpoint inhibitors in colorectal cancer	4
1.3 Limitations of immune checkpoint therapy	5
1.4 Predictive biomarkers for response to immune checkpoint therapy	6
1.5 Immune cell accumulation and predictive value	9
1.6 CD112R	9
1.6.1 Structure, function, and expressing cell types	9
1.6.2 Ligands and interaction network	10
1.6.3 CD112R expression in human and mouse	11
1.6.4 Prognostic relevance of CD112R in neoplasms	12
1.6.5 Clinical trials	12
1.7 Multiplex-Fluorescence-Immunohistochemistry	12
2. Material and Methods	14
2.1 Colorectal cancer large sections	14
2.2 Colorectal cancer tissue microarrays	14
2.3 Representativity of immune oncology study in TMA format	17
2.4 Cell culture, transfection of CD112R over-expressing HeLa reference cell line, and reference cell line TMA construction	18
2.5 Multiplex fluorescence immunohistochemistry	19
2.6 Deep learning-based digital image analysis approach	19
2.7 Statistical analysis	22
3. Results	24
3.1 Expression profile of CD112R and PD-1 on CD8 ⁺ T-cells	24
3.3 Upregulation of CD112R and PD-1 on CD8 ⁺ T-cells in T-cell niche	27
3.4 CD112R and PD-1 upregulation on CD8 ⁺ Ki67 ⁺ T-cells in tissue compartments and immune phenotypes	30
3.5 Prognostic relevance of spatial niche information	33
4. Discussion	36
5. Summary	40
6. Zusammenfassung	41
7. Abbreviations	42
8. List of Figures	43
9. List of Tables	44
10. References	45

11. Acknowledgments	55
12. Curriculum Vitae	56
13. Eidesstattliche Versicherung.....	57

1. Introduction

1.1 Historic development of immune checkpoint therapies

Currently, cancer treatment comprises a variety of different approaches, of which surgery, radiotherapy, and chemotherapy are dominating the field of cancer treatment. However, these cancer treatments are not specific for the cancer cells and thus they are accompanied by a high degree of side effects. Cancer immunotherapy has revolutionized anticancer therapeutics by restoring the preexisting anti-cancer immune response. Indeed, a great number of immunotherapy drugs have been successfully used in the clinic, effectively inhibiting tumor growth, maintaining immune homeostasis, and prolonging patient survival with minimal adverse effects (Kennedy and Salama, 2020). Given the emerging importance of immunotherapy, in 2018 James Allison and Tasuku Honjo were awarded with the Nobel Prize in Medicine or Physiology for their extraordinary contributions to the field of immunotherapy.

The spectrum of cancer immunotherapies is broad. Generally, immunotherapies are aiming for a reactivation of the immune system against malignant cells. The immunotherapy strategies include cancer vaccines, lymphokines, cell-mediated therapies like chimeric antigen receptor (CAR) T-cell therapy, and immune checkpoint blockade: For example, dendritic cell therapy has achieved a high efficacy in pancreatic cancer, by using short peptides or tumor lysates in combination with adjuvants (e.g., GM-CSF) to induce dendritic cells to present antigens (Palucka and Banchereau, 2013, Lutz et al., 2011). In addition, CAR engineered T-cells, which are immune cells isolated from cancer patients and modified to gain a new ability for specific proteins to effectively destroy tumor cells, have generated impressive efficacy against B-cell malignancies (Sermer and Brentjens, 2019).

Immunotherapies were developed based on the concept that malignant cell eventually gain immune escape mechanisms to evade anti-tumor immune reaction (Chen and Mellman, 2017). The immune system plays a critical role in immunosurveillance by detecting the tumor's aberrant antigen and initiating innate and adaptive immune responses to eradicate tumor cells: For instance, tumor cells release cytokines that act as ligands which activate negative regulatory pathways to consequently suppress immune responses (Chen and Mellman, 2017). Also, malignant cells become resistant to an immune induced apoptosis by tyrosine kinase mutations or IFN γ -receptor alterations (Dunn et al., 2002). Hence, cancer cells may survive during the recognition and elimination process. Consequently, the resistance to antitumor immune response allows tumor cells to exponentially grow and spread (Schreiber et al., 2011). Multiple mechanisms have been proposed to explain how the evasion of cancer cells occurs, including low immunogenicity and inhabitation of cytokine production

(Dunn et al., 2002) . Activation of key molecules that restrain immune response (also known as immune checkpoints) is considered to be one of the most indispensable components of tumor escape, which can inhibit T-lymphocyte activation and enhance the immune tolerance of tumor cells (Bagchi et al., 2021). Immune checkpoint inhibitory therapies benefit from the establishment of predictive biomarkers to assist oncologists finding constructive therapies for their patients, to select patients who would benefit from such therapy regimen, and to limit side effects (Gibney et al. 2016). Among these immune checkpoint molecules, programmed cell death protein 1 (PD-1), programmed cell death-ligand 1 (PD-L1) and cytotoxic T-lymphocyte-associated antigen 4 (CTLA-4) has been identified as a driver of tumor's immune evasion strategies and thus provide a promising target for inhibitory antibodies directed against these immune checkpoints (Bagchi et al., 2021) .

A new era of immunotherapy is targeting the immune checkpoint receptors to inhibit immune evasion mechanisms which hamper the anti-cancer immune reaction. Over the past few decades, tremendous progress has been made in immune checkpoint therapy (Couzin-Frankel, 2013). Anti-CTLA4, anti-PD-1, and anti-PD-L1 immune checkpoint inhibitors have shown remarkable clinical responses in a large fraction of patients across several different tumor entities, such as a high response rate to anti-PD-1 therapy in malignant melanoma (Kluger et al. 2017, Hodi et al., 2010) or to anti-PD-L1 therapy in advanced solid tumor types (Patnaik et al. 2020). Since the US Food and Drug Administration (FDA) approval of ipilimumab in 2011, which is directed against the CTLA-4 checkpoint, multiple immune checkpoint inhibitors have been approved for cancer therapy (Hargadon et al., 2018). To date, numerous clinical trials have been conducted to assess the efficacy and practicability of immune checkpoint inhibitors as monotherapy or combinatorial strategies. It has been shown that immune checkpoint therapy has become one of the most emerging fields in immune oncology.

1.2 Immune checkpoint inhibitors in colorectal cancer

Prior to the development of immune checkpoint therapy, solid tumor immunotherapy was mostly ineffective (Robert, 2020). Traditional immunotherapies like vaccines showed limited benefits and severe adverse effects (Rosenberg et al., 2004). However, immune checkpoint therapy has formed a new landscape in the field of cancer immunotherapy. In addition, a phase 2 clinical trial demonstrated that pembrolizumab therapy (PD-1 blockade) can result in durable antitumor immune responses in colorectal cancer patients with microsatellite instability and/or mismatch-repair deficiency (MSI/dMMR) (Le et al., 2015). Currently, immune checkpoint inhibitors including pembrolizumab, nivolumab (anti-PD-1), and ipilimumab (anti-CTLA-4) have been approved by the FDA for MSI-high/dMMR cancers regardless of the primary tumor locations. Of note, colorectal cancer is well known for its high tumor mutational burden and

thus a high degree of immunogenic neoantigens in the tumor microenvironment, that drives a strong infiltration by tumor-specific cytotoxic T-lymphocytes (TILs) (Yarchoan et al., 2017). Thus, these characteristics indicate that MSI/dMMR colorectal cancers are characterized by a preexisting anti-cancer immune response.

However, MSI/dMMR represents just a small part of colorectal cancers (14%) (Cohen et al., 2020). Thus, the majority of colorectal cancer, that exhibits unsatisfying responses to monotherapy, is microsatellite stable and mismatch-repair proficient (MSS/pMMR), displays a low level of tumor mutational burden, a lack of tumor-infiltrating lymphocytes (TILs), and an immunosuppressive status of the tumor microenvironment (Cohen et al., 2020). Given that immune checkpoint monotherapy showed limited efficacy in MSS/pMMR colorectal cancers, the combination treatment, such as the combination of PD-1 and CTLA-4 inhibitors, might elicit synergistic anti-tumor effects and provide novel insights for MSS/pMMR colorectal cancers. Phase 2 and 3 trials are currently being conducted to further investigate the potency of combined immune checkpoint therapies in colorectal cancer (Overman et al., 2018). In a recent phase 2 study (NCT02060188), response and a prolonged progression-free as well as overall survival were observed in an MSS/pMMR colorectal cancer treated with anti-PD-1 combined with anti-CTLA-4 therapy (Overman et al., 2018). Identifying alternative combinations with other modulating agents might improve the response to immune checkpoint inhibitors in colorectal cancers. Taken together, MSS/pMMR colorectal cancer is an arduous challenge for immune checkpoint therapy, requiring a thorough understanding of the tumor microenvironment and the relationship between immune cells and tumor cells.

1.3 Limitations of immune checkpoint therapy

Despite the success of immune checkpoint therapy in some advanced and therapy refractory human cancers, only a small fraction of patients (ranging from 10% to 30%) achieves benefits in most cancers such as non-small cell lung cancer, urothelial bladder cancer, and melanoma (Ribas and Wolchok, 2018). For example, head and neck cancer patients treated with pembrolizumab (anti-PD-1) or nivolumab (anti-PD-1) showed a 13.3% or 16% immune response (Johnson et al., 2020, Mehra et al., 2018). The melanoma patients treated with Ipilimumab (anti-CTLA-4) exhibited a 16.8% of immune response (Larkin et al., 2015). Of note, colorectal cancer patients with MSS/pMMR PD-1 immune checkpoint therapy failed to achieve immune response to PD-1 blockade (Le et al., 2015). In contrast some other entities such as Hodgkin's lymphoma higher overall response rates – up to 87% – were observed (Meti et al., 2018). The mechanisms of low-responsiveness have been thoroughly investigated and many factors have been found to be associated with it, such as PD-L1 expression, tumor mutational burden, Tumor-infiltrated lymphocytes (Duffy and Crown, 2019). Currently, dual blockade of

immune checkpoints seems to be a promising approach to improve immune response (Hellmann et al., 2018).

In addition to the generally low immune response rate of immune checkpoint therapy, it is also frequently linked to distinct toxicities that are well known as immune-related adverse events (irAEs) (Larkin et al., 2015). With the increasing use of immune checkpoint inhibitors, the incidence and severity of irAEs also seem to be rising, as some reports indicate a 10-30% frequency of severe irAEs (Spain et al., 2016). Any organ can be affected by irAEs, but irAEs vary between patients and immune checkpoint inhibitors and typically affect the gastrointestinal tract, skin, lung, endocrine, and central nervous system (Postow et al., 2018). Even though the occurrence of irAEs suggests a favorable prognosis for some patients receiving immune checkpoint therapy, serious irAEs can also potentially lead to treatment termination and fatal outcomes. Additionally, life-threatening irAEs can appear in the early stage of treatment, typically three months after treatment (Chan et al. 2020), particularly for patients treated with combinatorial therapies: In a meta-analysis, patients receiving a PD-1 combined with a CTLA-4 blockade experienced irAEs onset of fatal outcomes within the first 14.5 days of treatment (Wang et al., 2018). Furthermore, severe toxicities usually require early drug intervention, such as corticosteroids, to prevent irreparable consequences, which may also affect the efficacy of the immune checkpoint therapy (Arbour et al., 2018). Arbour et al. illustrated, that baseline corticosteroid at the onset of immune checkpoint therapy was correlated with poor outcomes in patients with non-small-cell lung cancer (Arbour et al., 2018). Therefore, it is urgent to explore biomarkers predicting the efficacy of immune checkpoint therapy and the occurrence of irAEs to achieve substantial therapeutic benefits.

1.4 Predictive biomarkers for response to immune checkpoint therapy

Predictive markers are biologic surrogates reflecting the likelihood of response to treatment before the initiation of therapy. A series of predictive biomarkers based on the tumor microenvironment (TME) and tumor biology have proven to predict the clinical outcome of patients treated with immune checkpoint inhibitors (Gibney et al., 2016).

The role of PD-L1 expression on tumor cells and immune cells has been extensively investigated, owing largely to the crucial role of PD-L1 in suppressing immunogenicity. A wide range of prospective studies has shown that elevated PD-L1 expression in the TME is correlated with clinical efficacy (Buder-Bakhaya and Hassel, 2018, Diggs and Hsueh, 2017). There is some evidence that patients who received a durvalumab therapy (PD-L1 blockade) with above 25% PD-L1 expression on tumor cells had preferentially objective responses (Antonia et al., 2018). Subsequent trials have demonstrated that a PD-L1 positive TME is a

prerequisite for anti-tumor responses, which is linked to an improved progression-free survival and overall survival irrespective of therapy types which can be productively used to stratify patients for a PD-L1/PD-1 therapy (Borghaei et al., 2015, Garon et al., 2015). As yet, the FDA has approved a variety of commercial anti- PD-L1 agents and diagnostic assays to quantify PD-L1 expression (Ma et al., 2016). However, as the research progressed, the limitations of detecting PD-L1 in IHC were emphasized: Various agents and testing platforms with different thresholds of PD-L1 positivity (ranging from 1% to 50%) as well as scoring methods cause difficulties in the assessment of PD-L1 expression (Arora et al., 2019). Several studies suggested that PD-L1 alone might not be an adequate biomarker to predict the responsiveness to therapy (Hodi et al., 2018). Accordingly, an average of 10% of PD-L1 negative patients responded to immune checkpoint inhibitors and achieved tumor regression to a certain extent (Patel and Kurzrock, 2015). Furthermore, due to the heterogeneous expression of PD-L1, the representative biopsy specimen may not truthfully reflect the PD-L1 expression throughout the entire tumor parenchyma. Hence, PD-L1 expression is a powerful biomarker for predicting response to immune checkpoint inhibitors, but it needs further studies to extend the sole analysis of PD-L1 by other biomarkers to improve the predictive performance.

Microsatellite instability refers to functional defects of mismatch repair which are capable of rectifying frameshift mutation associated with DNA replication and results in the accumulation of short tandem repetitive DNA sequences (termed microsatellites) in the genome (Lin et al., 2020). Patients with the occurrence of MSI/dMMR, which increases the number of mutations and neoantigens, have greater probabilities to attract lymphocytes: Thus, it is intuitive that MSI/dMMR can serve as an adequate predictor for response to immune checkpoint therapy. According to Le et al., 40% of colorectal cancer patients with MSI/dMMR had a significant objective response to pembrolizumab, compared to 0% of colorectal cancer patients with MSS/pMMR (Le et al., 2015). Several studies have also demonstrated that patients with MSI/dMMR benefitted from a nivolumab therapy, as well as a combined immune checkpoint therapy with nivolumab and ipilimumab (Overman et al., 2017, Overman et al., 2018). Identifying MSI/dMMR as a predictive biomarker was a breakthrough for colorectal cancer patients: However, MSI/dMMR is only a small fraction of patients (14% of colorectal cancer, 10% of breast cancers, \leq 2% of non-small cell lung cancers, and esophageal cancers), meaning that MSI/dMMR cannot be universally applied to most cases (Baretti and Le, 2018). Thus, a more broadly applicable marker to predict patient prognosis is urgently needed.

Given that MSI represents a well-established marker for response to immune checkpoint therapy, it is intuitive that the mutational burden – displaying the total number of coding mutations per megabase of the tumor DNA – has become also a predictive biomarker for response to immune checkpoint therapy and patients' outcome (Boyiadzis et al., 2018). The

mutational burden represents the connection between the field of genetics and the likelihood of the successful response to immune checkpoint inhibitors in the field of immune oncology. The mutational burden leads to tumor specific epitopes (termed neoantigens) which are recognized as foreign peptides by tumor infiltrating CD4⁺ and CD8⁺ T-cells (Riaz et al., 2016). It is intuitive that tumors with a higher mutational burden are more likely to express and present neoantigens, consequently inducing a stronger immune response (Lauss et al., 2017, Samstein et al., 2019). However, there is evidence that TMB might not be an adequate biomarker. A comprehensive study revealed that lung cancer patients with high TMB achieved nonsignificant prolonged overall survival from ipilimumab and nivolumab therapies (Hellmann et al., 2018). Moreover, Zhou et al., found that colorectal cancer patients with a low mutational burden showed a higher overall survival (Zhou et al., 2021). Although the tumor mutational burden provides important complementary information for the immune response to immune checkpoint therapy, the role of mutational burden as a predictive biomarker remains elusive.

Another predictive biomarker represents the density of TILs, which is associated with improved immunotherapeutic response regardless of immune checkpoint inhibitor therapy (Duffy and Crown, 2019). Based on the distribution pattern of leucocyte infiltration, immune phenotypes can be characterized: The immune tumor microenvironment can be characterized as an inflamed and non-inflamed immune phenotype (Chen and Mellman, 2017). In the addition, the non-inflamed phenotype can be differentiated in an immune-excluded and immune-deserted phenotype (Chen and Mellman, 2017). The immune-inflamed phenotype refers to the high infiltration of lymphocytes across all components in the tumor microenvironment, in which active immune responses are seen (Mandelkow et al., 2019). The immune-excluded phenotype is classified by immune cells that are predominantly located at the invasive margin and cannot penetrate the tumor parenchyma so that the center of the tumor appears rather non-inflamed (Chen and Mellman, 2017). Furthermore, the immune-desert phenotype is characterized by the absence of lymphocytes in both, the center of tumor and at the invasive margin (Havel et al., 2019). To quantify the status of tumor infiltrating lymphocytes, an immunoscore has been proposed based on the density of T-cells located at the invasive margin and the center of the tumor, which was associated with longer disease-free survival and was considered to be an independent prognostic factor (Galon et al., 2006). Another study revealed that an immunoscore was superior to MSI as a predictive biomarker for predicting patients' disease-specific recurrence and survival in colorectal cancer, indicating that fundamental characteristics of TILs may be fundamental for the understanding of the tumor microenvironment and could be a guidance for clinicians using immune checkpoint therapy (Mlecnik et al., 2016).

1.5 Immune cell accumulation and predictive value

Although the overall density of immune cells has been studied widely, local accumulations, which play a key role in the immune escape mechanism, remains unclear (Jansen et al., 2019). Evidence suggests that the presence of locally enriched immune cells serves as a novel prognostic biomarker that can facilitate TIL recruitment, rather than the assessment of the overall density (Di Caro et al., 2014). Numerous studies have evaluated the role of tertiary lymphoid structures, ectopic lymphoid tissues with high densities of TILs, macrophages, and dendritic cells distributed across different tumor types, and have consistently found an association between high numbers of tertiary lymphoid structures and favorable survival (Sautes-Fridman et al., 2016). In addition, Patel et al., showed that the microenvironmental niche consisting of PD-L1⁺ Hodgkin Reed-Sternberg cells and macrophages were enriched along with CTLA-4⁺ PD-1⁻ T-cells (Carey et al., 2017). Moreover, Jansen et al., have revealed that stem-like (TCF⁺CD8⁺) T-cells are closer to the aggregations of antigen-presenting cells (APCs) and that the development of immune niches was associated with T-cell- and vascular infiltration (Jansen et al., 2019). These facts suggest that the immune niche was an important driving factor for the anti-cancer immunity (Jansen et al., 2019). With the evidence presented above, it is possible that the characteristics and features of local accumulated immune cells in the TME are the key to understand the morphological mechanism of tumor escape. All these findings raise a profound question of how immune checkpoints perform within immune niches.

1.6 CD112R

1.6.1 Structure, function, and expressing cell types

CD112R (PVRIG) is a transmembrane protein consisting of an extracellular immunoglobulin V domain, a transmembrane domain, and an intracellular domain (Zhu et al., 2016). CD112R was originally named "poliovirus receptor-associated immunoglobulin structural domain containing" (PVRIG) to indicate the structure of the protein: After identifying the protein as a novel inhibitory immune-checkpoint receptor, PVRIG was named CD112-receptor (CD112R) to emphasize the relationship between PVRIG and CD112 (Zhu et al., 2016). Interestingly, the intracellular structural domain of CD112R has two tyrosine residues, one of which is an immunoreceptor tyrosine-based inhibitory motif (ITIM) that can be phosphorylated for activation signal transduction (Billadeau and Leibson, 2002). Zhu and colleagues revealed that CD112R inhibits T-cell receptor (TCR) -mediated activation of nuclear factor of activated T-cells (NFAT) and attenuate or terminate immune responses (Zhu et al., 2016). These results have been successively confirmed by another study in which CD112R-deficient mice had enhanced immune responses and tumor regression *in vivo* due to the inhibitory effect of interaction between CD112R and Nectin-2 on cytokine production of T-cells (Murter et al., 2019). Moreover, CD112R is associated with NK cell suppression. Xu et al., discovered that

PVR-like (e.g., TIGIT and CD112R) ligand can lead to NK cell internalization and an increasing NK cell cytokine production by blocking TIGIT and/or CD112R (Xu et al., 2017).

1.6.2 Ligands and interaction network

Nectin or nectin-like molecules expressed on APC or tumor cells competitively or synergistically bind to receptors like CD112R, which belongs to the immunoglobulin superfamily receptors, including T-cell immunoglobulin and ITIM domain (TIGIT), CD226/DNAM-1, and CD96/TACTILE. Nectin proteins contain four molecules including nectin-1 (PVRL1/CD111), nectin-2 (PVRL2/CD112), nectin-3 (PVRL3/CD113), and nectin-4 (PVRL4). Nectin-like proteins contain five molecules (necl-1-5), of which necl-5 (PVR/CD155) plays a key role in the network of interactions.

Poliovirus receptor (PVR) has been reported as a potential target for antitumor treatment (He et al., 2000, Bowers et al., 2017). Although PVR is not fully understood, many studies have shown that it is a stress-induced transmembrane ligand and a direct marker of malignancy progression, shown by an activation of the Shh pathway (abnormally activated in malignant tumors) and the ATM/ATR pathway (generally found in precancerous lesions) due to upregulation of PVR (Solecki et al., 2002, Soriani et al., 2009). Mechanically, PVR can bind to TIGIT, CD226, and CD96. The binding of PVR to different receptors can prompt reverse immune responses, including interactions with CD226 enhancing T-cell cytotoxicity and cytokine production as well as interactions with TIGIT conversely leading to suppression of immune responses: But the function of the interaction between PVR and CD96 remains unknown (Gorvel and Olive, 2020). However, PVR binds TIGIT with highest affinity, and binds TIGIT also through homodimerization of CD226, which leads to the overall inactivation of T-cells (Chauvin and Zarour, 2020). Thus, inhibition of TIGIT would be an intuitive strategy to reactivate T-cells via the PVR network. A number of Phase 1 and Phase 2 clinical trials with TIGIT alone or in combination are currently in progress (Sanchez-Correa et al., 2019, Rodriguez-Abreu et al., 2020, Ambrosi et al., 2019) and an anti-TIGIT antibody (Tiragolumab) in lung cancer patients has shown prolonged progression-free survival (Harjunpaa and Guillerey, 2020, Rodriguez-Abreu et al., 2020). Notably, TIGIT also binds to nectin-2 (PVRL2/CD112), but with less affinity compared to the PVR-TIGIT axis (Harjunpaa and Guillerey, 2020). Given the redundant function of PVR in regulating immune responses, nectin-2 (PVRL2/CD112) may also be a promising target for immunotherapy.

Nectins are adhesion molecules involved in the growth and development processes of various tissues as well as viral infections and cancers (Takai et al., 2008). Nectin-2 (PVRL2/CD112) is expressed by tumor cells and a few myeloid cells (e.g., APC) (Takai et al., 2008). In addition,

PVRL2 can also bind to CD226 and TIGIT, initiating stimulation or suppression of the immune response. However, the affinity of CD112R-PVRL2 was significantly higher than the one of TIGIT-PVRL2 and CD226-PVRL2. A recent study showed that the inhibitory effect of PVRL2 is transmitted through CD112R rather than TIGIT (Whelan et al., 2019). Moreover, several studies showed that the blockade of CD112R can effectively improve the cytotoxicity of CD8⁺ T-cells (Gorvel and Olive, 2020, Murter et al., 2019). Of note, the CD112R-PVRL2 axis has become an emerging inhibitory pathway that offers new opportunities for immunotherapy to synergize with PD-1/PD-L1 blockade therapies. Nevertheless, only a limited number of trials and studies are investigating the CD112R-PVRL2 pathway, and many questions still need to be answered to unveil the mechanism of this pathway.

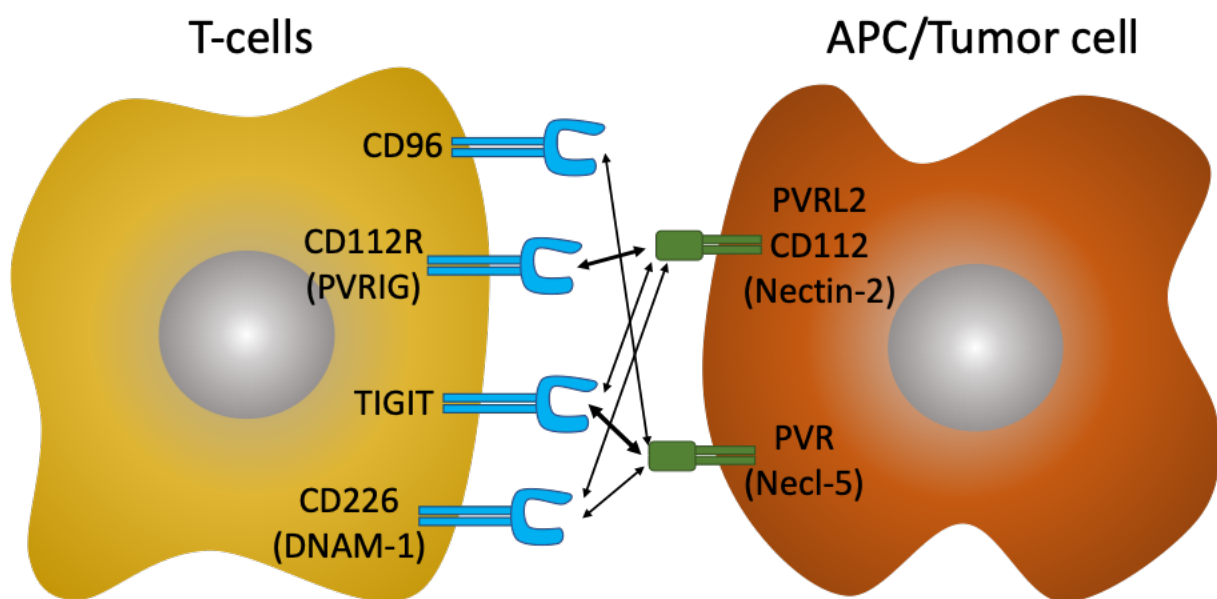


Figure 1: Interaction network between the immune checkpoint receptors (blue) and their ligands (green). The size of the arrows indicates the affinity of the interaction.

1.6.3 CD112R expression in human and mouse

CD112R is expressed on CD4⁺ and CD8⁺ T-cells, NKT-cells, and natural killer (NK) cells (Whelan et al., 2019, Zhu et al., 2016, Xu et al., 2017). Zhu et al. found a detectable expression of CD112R in most T-cells and NK cells analyzing the mRNA expression level. Another study showed that CD112R transcripts were enriched in NK and NKT-cell, but not detectable in B-cells in mouse models (Murter et al., 2019). Whelan et al. confirmed that CD8, CD4, and NK cells express CD112R (Whelan et al., 2019). Thereby the highest CD112R expression on CD8⁺ and CD4⁺ T-cells was detected in ovarian, kidney, lung, endometrial, and breast cancers, while the highest CD112R expression on NK⁺ cells were detected in prostate cancer (Whelan et al., 2019). Moreover, CD112R was co-expressed with other immune checkpoints (e.g., TIGIT and PD-1), suggesting an exhausted status of such T-cells (Whelan et al., 2019). Blockade of

CD112R and/or TIGIT can effectively enhance the immune response triggered by NK cells (Xu et al., 2017).

1.6.4 Prognostic relevance of CD112R in neoplasms

The prognostic relevance of CD112R might be pivotal for a deeper insight in this immune checkpoint. However, the current reports of CD112R are so sparse that there is very limited knowledge of the prognostic role of CD112R: Qiao et al., and Tang et al., reported that elevated CD112R gene expression was significantly associated with longer overall and relapse-free survival in hepatocellular carcinoma (Qiao et al., 2019, Tang et al., 2019).

1.6.5 Clinical trials

As yet, there are phase 1 (NCT03667716) and 2 clinical trials (NCT04570839) using anti-CD112R therapy ongoing. These studies are assessing the clinical efficacy of COM701, a novel humanized CD112R inhibitor, as a monotherapy compared to a combination therapy with nivolumab for patients with advanced solid malignancies. Preliminary results reported that 69% of patients in the COM701 monotherapy cohort and 75% of patients in the combination therapy cohort – combined with an anti-PD-1 treatment – achieved clinical disease control (Sullivan et al., 2020b). This study demonstrated that COM701 was well-tolerated as both a stand-alone treatment and in combination with nivolumab in patients with a wide range of late-stage neoplasms. Notably, even in refractory tumor types (primary peritonitis and MSS/pMMR colorectal cancer), COM701 showed immunotherapeutic responses as monotherapy or in combination with nivolumab (Sullivan et al., 2020a). Moreover, adverse effects were tolerable: mainly fatigue, nausea, and anxiety appeared after treatment (Sullivan et al., 2020b). This study further evaluated the safety, tolerability, and preliminary antitumor activity of COM701 alone for patients with advanced neoplasms (Lentz et al., 2021). The results of the study exhibited the favorable tolerability and safety profile of COM701 (Lentz et al., 2021).

1.7 Multiplex-Fluorescence-Immunohistochemistry

Immunohistochemistry (IHC) is a qualitative and quantitative application using the principle of specific antibody binding to distinct molecules in formalin fixed and paraffin embedded tissues to visualize the target proteins via a detection system for the specific antibody binding. Since the 1970s, the conventional bright field immunohistochemistry (bfIHC) has been applied to pathological diagnostics, which is an essential tool for tumor classification and prognosis assessment in routine clinical pathology. However, the detection of only a single marker might be insufficient in some situations (e.g., biopsies with only a limited amount of tissue). To address this issue, in multiplex fluorescence immunohistochemistry (mfIHC) the detection

system of the primary antibodies allows the characterization of up to 40 biomarkers simultaneously or sequentially (Goltsev et al., 2018).

There are several mFIHC staining techniques using sequential antibody staining or sequential fluorochrome binding. The mFIHC with the strongest fluorescence signal is the tyramide signal amplification (TSA) method, which is a class of enzymatic assays that use horseradish peroxidase (HRP) for high-density in situ labeling of target proteins or nucleic acids (Stack et al., 2014). Like conventional immunohistochemistry development, the TSA technique also uses HRP-labeled secondary antibodies. HRP catalyzes the addition of a fluorescein substrate to the system to generate an activated fluorescent substrate, which can covalently bind to the tyrosine on the antigen, resulting in stable binding of fluorescein on the tissue sample. Afterwards, the bound antibody is washed away, and the next primary antibody staining step using another fluorescein substrate can be performed. In contrast to this sequential antibody staining approach, the co-detection by indexing (CODEX) framework stains all primary antibodies at the same time which are detected by fluorochromes via specific DNA-barcodes hybridization sequentially along with multiple cycles of fluorochrome binding and imaging (Goltsev et al., 2018).

2. Material and Methods

2.1 Colorectal cancer large sections

In this study, two different colorectal cancer cohorts were used. The first cohort consisted of 20 large sections from colorectal cancer patients, whose tumor resection specimens were examined at the Institute of Pathology of the University Medical Center Hamburg-Eppendorf, were used in this study. All 20 cases were inspected by an experienced pathologists to ensure tissue integrity and diagnostic correctness. The median overall follow-up time of each patient was 15 months (range 1–36 months). The patient’s median tumor diameter was 46 mm (range 22-130 mm). All tissues were fixed in formalin and individually embedded in paraffin blocks. The Hematoxylin and Eosin staining (H&E) was performed to first display the structures of the tissues before multiplex fluorescence immunohistochemistry was applied. The construction of large sections for research purposes have been approved by local laws (HmbKHG, §12,1) and by the local ethics committee (Ethics commission Hamburg, WF-049/09). All work was performed in compliance with the Helsinki Declaration. (For patient characteristics of large section see Table 1)

Patients characteristics	No. of patients (%)	
	Study cohort on TMA (n=20)	Overall death among categories
Follow-up - no. (%)	20 (100.0%)	6 (30.0%)
Mean/median - months	20.1/15.0	-
Tumor diameter (mean/median) - mm	52.8/46.0	-
pT stage - no. (%)		
pT1	0 (0%)	0 (0%)
pT2	3 (15%)	0 (0%)
pT3	14 (70%)	5 (36%)
pT4	3 (15%)	3 (33%)
pN stage - no. (%)		
pN-	11 (55%)	2 (18%)
pN+	9 (45%)	4 (44%)
Vascular invasion - no. (%)		
Negative	10 (50%)	1 (10%)
Positive	10 (50%)	5 (50%)

Table 1: Patient characteristics are shown for the large section cohort.

2.2 Colorectal cancer tissue microarrays

Tissue microarrays (TMAs) are a classical pathological technique that arranges a large number of tissue cores accurately in the same paraffin-embedded block and allows to stain up to 600 patients at the same time within on experiment (Kononen et al., 1998, Sauter et al., 2003). The corresponding tissue samples were collected from the archives of the Institute of Pathology of

the University Medical Center, Hamburg-Eppendorf by an experienced pathologists to ensure the correctness of the diagnosis and the potential availability in the TMA. The TMAs were constructed from 4% buffered formalin fixed, paraffin embedded archived tissue samples. Briefly, a 0.6 mm core was taken from each patient's tumor-containing tissue block. The tissue punches were evenly distributed across the TMA blocks.

The second cohort of this study consisted of one TMA, which was manufactured from resection specimens of 522 colorectal cancer patients at the Institute of Pathology of the University Hospital of Basel. Raw survival data were obtained from the responsible physicians for all 522 patients. The median overall follow-up time was 58 months (range 1–152 months). The use of archived diagnostic left-over tissues for manufacturing of TMAs and their analysis for research purposes has been approved by local laws (HmbKHG, §12,1) and by the local ethics committee (Ethics commission Hamburg, WF-049/09). All work was performed in compliance with the Helsinki Declaration. (For patient characteristics of TMA see Table 2)

Patients characteristics	No. of patients (%)	
	Study cohort on TMA (n=522)	Overall death among categories
Follow-up - no. (%)	522 (100.0%)	334 (60.5%)
Mean/median - months	64.5/58.0	-
Age (median) - years	71.0	-
Tumor diameter (mean/median) - mm	51.7/50.0	-
pT stage - no. (%)		
pT1	17 (3.3%)	4 (23.5%)
pT2	67 (12.8%)	26 (38.8%)
pT3	355 (71.0%)	236 (66.5%)
pT4	69 (13.2%)	61 (88.4%)
Missing data	14 (2.7%)	-
pN stage - no. (%)		
pN-	255 (48.9%)	125 (49.0%)
pN+	246 (47.1%)	198 (80.5%)
Missing data	21 (4.0%)	-
Grade - no. (%)		
1	11 (2.1%)	2 (18.2%)
2	462 (88.5%)	300 (64.9%)
3	34 (6.5%)	24 (70.6%)
Missing data	15 (2.9%)	-
Histotype - no. (%)		
Adenocarcinoma	472 (90.4%)	302 (64.0%)
Medullary	4 (0.8%)	3 (75.0%)
Mucinous	35 (6.7%)	23 (65.7%)
Signet ring cell	2 (0.4%)	2 (100.0%)
Missing data	9 (1.7%)	-
Tumor localization - no. (%)		
Anal	12 (2.3%)	6 (50.0%)
Appendix	1 (0.2%)	1 (100.0%)
Ascendens	59 (11.3%)	38 (64.4%)
Cecum	76 (14.6%)	55 (72.4%)
Descendens	28 (5.4%)	17 (60.7%)
Rectosigmoid	31 (5.9%)	21 (67.7%)
Rectum	179 (34.3%)	119 (66.5%)
Sigmoid	87 (16.7%)	47 (54.0%)
Transversum	48 (9.2%)	29 (60.4%)
Missing data	1 (0.2%)	-
Vascular invasion - no. (%)		
Negative	364 (69.7%)	209 (57.4%)
Positive	144 (27.6%)	118 (81.9%)
Missing data	14 (2.7%)	-
Invasive margin - no. (%)		
Infiltrating	360 (69.0%)	251 (69.7%)
Pushing	146 (28.0%)	75 (39.0%)
Missing data	16 (3.1%)	-
Peritumoral lymphocytes - no. (%)		
Absent	385 (73.8%)	255 (66.2%)
Present	123 (23.6%)	72 (58.5%)
Missing data	14 (2.7%)	-

Table 2: Patient characteristics are shown for the TMA cohort.

2.3 Representativity of immune oncology study in TMA format

To further explore the representativity of the TMA method for CD8⁺ cytotoxic T-cell assessment, the large sections were used to model a virtual TMA: 50 virtual TMA cores were randomly allocated within the center of the tumor and the CD8⁺ density of every virtual TMA core was calculated (Figure 2). The data underlined that the TMA format – with 0.6 mm in diameter tissue cores – was an appropriate method for quantifying the CD8⁺ density in the tumor center which was also in line with earlier findings (Blessin et al., 2020). However, large sections might be superior for the analysis of T-cell niches compared to the analysis of 0.6mm TMA cores. Although the TMA method is a very robust and highly standardized tool for the analysis of tumor markers and abundant immune cells, the TMA format may not be adequate for rare immune cell subtypes.

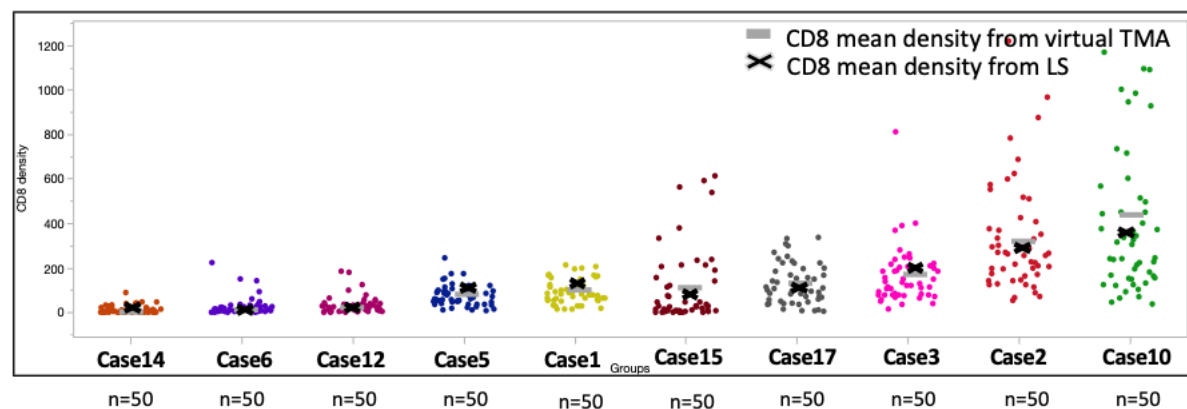
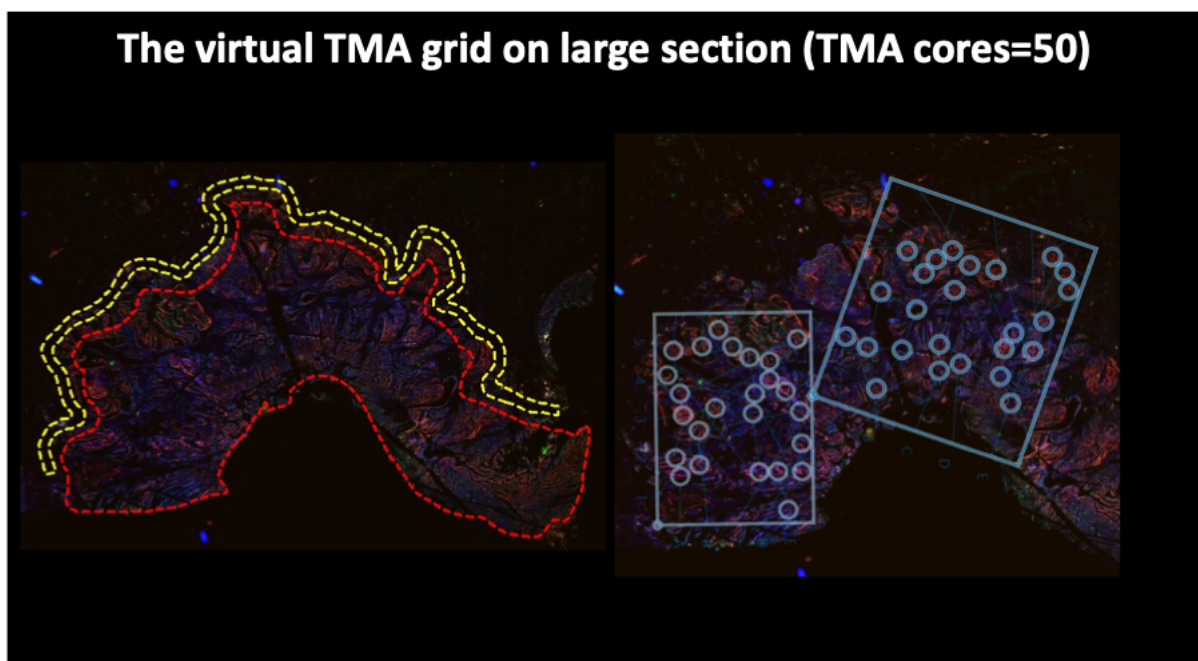


Figure 2: The representative multiplex fluorescence immunohistochemistry image of a large section is displayed. The virtual TMA grid (50 cores) is applied to mimic the TMA segmentation, one core represents one punch (top). The CD8⁺ density of each punch and overall density of the large section is calculated (bottom).

2.4 Cell culture, transfection of CD112R over-expressing HeLa reference cell line, and reference cell line TMA construction

2.4.1 Cell culture, transfection of CD112R over-expressing HeLa reference cell line

Human cervix epithelial carcinoma cells (HeLa) were maintained in DMEM (Dulbecco's Modified Eagles Medium, Gibco), complemented with 10% fetal bovine serum (FBS) and 1% penicillin-streptomycin (P/S). The HeLa cells were cultured in multi-layer cell culture flasks at 37°C and 5% CO₂. The construct encoding for CD112R (PVRIG) under control of the CMV promoter was acquired from Sino Biological Inc. (Beijing, China). The vector was transformed in competent *Escherichia coli* cells (One Shot™ Top10, ThermoFisher Scientific, Germany). The amplified plasmid was extracted by using the plasmid purification kit (Macherey-Nagel) according to the manufacturers' instructions. After the DNA product was diluted with distilled, sterile water, the final concentration was measured with a NanoDrop-1000 spectrophotometer (PeqLab). The construct was finally used for transfection. In brief, 3x10⁶ HeLa cells were seeded on sterile petri dishes cultured in 20 mL of DMEM supplemented with 10% FBS and 1% P/S and incubated at 37°C to achieve around 50 - 60% of confluence. After 24 h the cells were washed with PBS (1x) and 8 mL fresh medium was added followed by transfection with the CD112R plasmid DNA using JetPEI DNA Transfection reagent (Polyplus-transfection S.A., BIOPARC, Illkirch France) according to the manufacturers' instructions.

2.4.2 Reference cell line TMA construction

After 24h the cells were harvested with 4 mL Accutase™ and centrifuged at 1000 x g for 5 min at room temperature. The cells were embedded in agarose followed by a formalin fixation and lastly implanted in a paraffin block. As a negative control HeLa cells without transfection were added. Both cell lines were represented in duplicate and added to the reference TMA. Additionally, seven tonsil tissues (including follicular and interfollicular) from healthy donors were also be integrated to the reference TMA according to the previously mentioned steps.

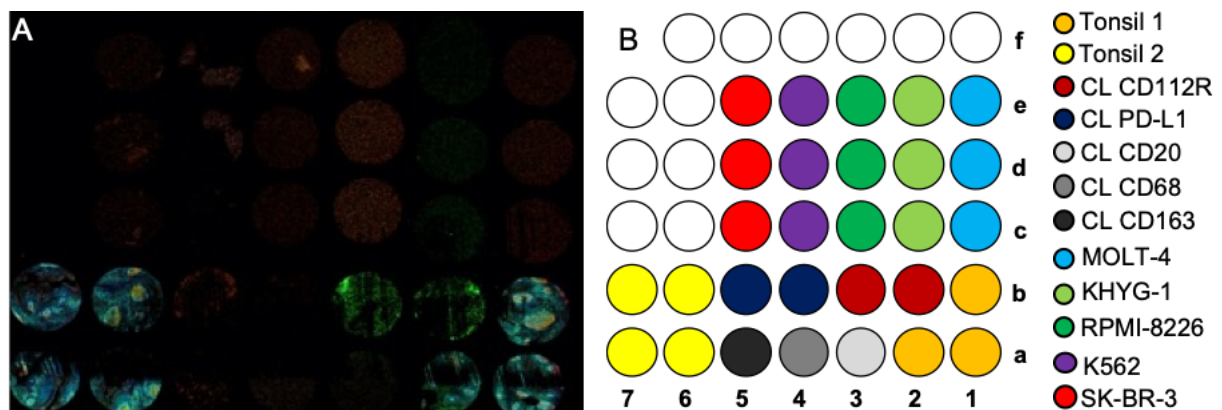


Figure 3: The representative reference TMA image (A) and reference TMA layout (B) are displayed.

2.5 Multiplex fluorescence immunohistochemistry

Freshly cut 4- μ m consecutive tissue sections were used for multiplex fluorescence immunohistochemistry analyses. The specificity of the anti-CD112R antibody clone DIA-R12 (Dianova, Hamburg, Germany) was validated by Western blot, Enzyme-linked immunosorbent assay (ELISA), and pre-absorption of the primary antibody with CD112R protein. In addition, the staining pattern of this particular anti-CD112R antibody was extensively evaluated in normal lymphatic tissue and cancer earlier (Blessin et al., 2021b). For fluorescence multiplex IHC, the OPAL dye kit (Cat. # NEL811001KT, AKOYA Biosciences, Menlo Park, California, United States) was used. Details on the used antibodies, antibody retrieval procedures and OPAL dyes are given in Table 1. The experimental procedure was performed according to the manufacturer's instructions (AKOYA). Slides were initially boiled in an autoclave (30 minutes at 100-120°C in pH9 buffer) for antigen retrieval. One cycle of antibody staining included peroxidase blocking, application of the primary antibody, detection with a secondary HRP-conjugated antibody, fluorescence dye detection, and removal of the bound antibodies by microwave treatment (5 minutes at 100°C and 5 minutes at a mean temperature of 93°C). This cycle was repeated three times for the remaining antibodies. Slides were subsequently counterstained with diaminodino-2-phenylindole (DAPI) and mounted in antifade solution.

Antibody target	Identifier	AR (pH value)	Dilution	Staining position	Opal dye
Ki67	MSVA, Clone: MSVA-267R Cat#: 2843-267R	9.0	1:50	1	520
CD112R	Dianova; Clone: R12 Cat#: DIA-R12	7.8	1:500	2	570
PD-1	Abcam; Clone: EPR4877(2) Cat#ab137132	7.8	1:150	3	690
CD8	DAKO; Clone: C8/144B Cat#IR623	9.0	RTU	4	780

(MSVA: MS Validated Antibodies GmbH, AR = antigen retrieval; Cat# = Catalogue number; RTU = Ready to use)

Table 3: List of used antibodies, antigen retrieval (AR), dilutions, and Opal dyes for multiplex fluorescence immunohistochemistry.

2.6 Deep learning-based digital image analysis approach.

A representative example of the image analysis workflow has been described earlier (Blessin et al., 2021b, Blessin et al., 2021a). In brief, digital images of mflHC stained slides were acquired with a Leica Aperio VERSA 8 automated epifluorescence microscope and a Zeiss Axio Scan.Z1 slide scanner. Image analysis was performed using a U-net deep learning algorithm for cell detection, cell segmentation and intensity measurement of the used fluorophores (range 0-255, i.e., a continuous numerical value indicating the fluorescence signal strength), which we have trained and validated using python version 3.8 (Foundation, 2021)

and the Visiopharm software package (Hoersholm, Denmark). Annotated cells from more than 100 different tumor entities were used to train the cell detection U-Net. The intensity of each fluorochrome was recorded as raw intensity for every individual cell. Only staining intensities exceeding a predefined threshold were considered “positive”. The threshold was individually selected in a multi-step procedure for each marker (CD8, Ki67, CD112R, PD-1) according to the following procedure: The fluorescence intensity of each marker was measured in 50 to 200 cells with expected lack of expression and the value of the cell with highest “false positive” measurement was used as provisional cut-off value for positive expression. This value was reconsidered by way of plotting the intensity values of the measured markers in scatter plots with logarithmic scale using R (R-Core-Team, 2021) to perform an additional gating step (i.e., identification of homogenous cell populations that share a particular function), which is well known from flow cytometry (Bashashati and Brinkman, 2009). The measured threshold from these two validation steps was reviewed by a trained pathologist across multiple tissue types in a test-TMA before the cut-off has been used.

2.6.1 Large section analysis

In order to compare CD112R and PD-1 expression levels between different large sections, the raw CD112R intensity was normalized to a CD112R over-expressing HeLa reference cell line and the raw PD-1 intensity was normalized to follicular T-helper cells (Blessin et al., 2019) in the germinal centers of healthy human reference tonsils. Accordingly, two spots of the reference cell line and seven spots of the reference tonsils measuring 2mm in diameter were placed on each slide and the mean raw intensity of the reference cells was set to 100% for each immune checkpoint receptor individually. The relative expression was then calculated as the percentage of mean raw intensity of the test cells in relation to the 100% mean raw intensity measured in the reference cells.

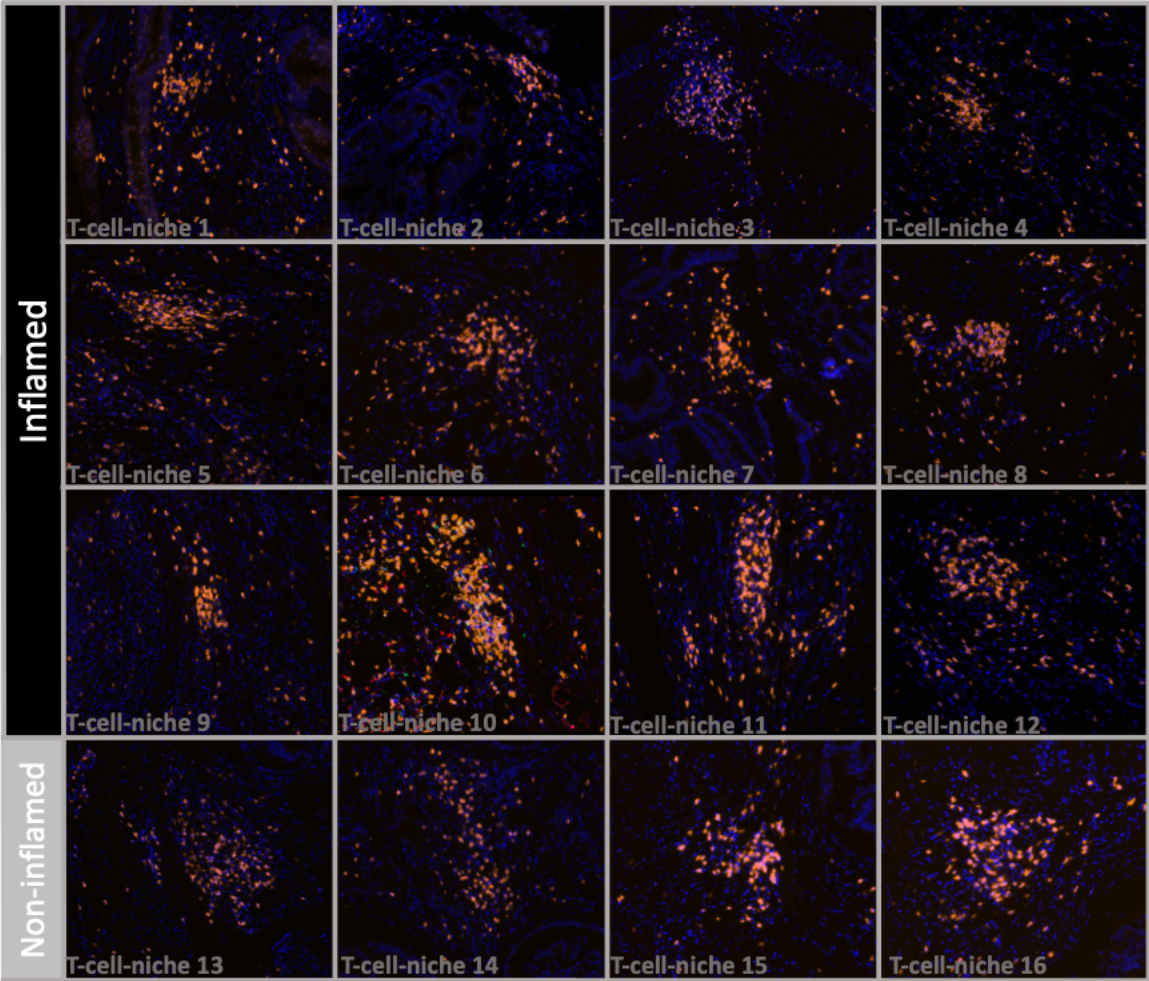
1. The center of tumor and invasive margin were defined for 20 large sections. Two experienced pathologists were trained to annotate the invasive margin and the center of tumor according to the following principles. A boundary line was first drawn between the stroma and the tumor, and the invasive margin was then defined according to the boundary line extending 50 μ m to the tumor and 300 μ m to the stroma, the center of tumor was defined as a tumor parenchyma away from the borderline.

2. T-cell niche was detected by the custom algorithm. Dense accumulations of CD8⁺ cytotoxic T-cells were identified as CD8⁺-T-cell niches by statistical analysis and histopathological review (Figure S1). The number of cells close to the index cell were quantified and normalized by the area around the index cell using custom R scripts (R-Core-Team, 2021) to calculate the local density of cells close to the index cell. A 20 μ m radius (around the center of the index cell) appeared to be most accrued for CD8⁺ T-cell niche identification (Figure 2). Given the fact that

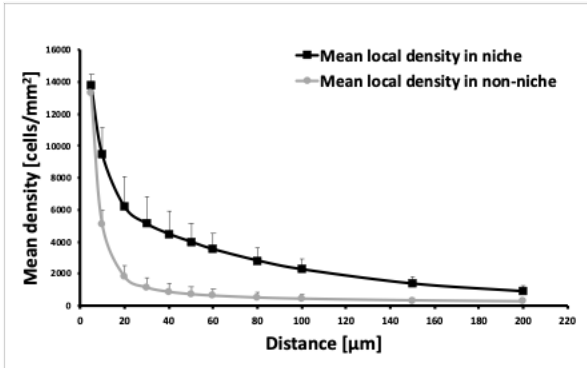
the local density of other T-lymphocyte subsets was found elevated along with the local CD8⁺ T-cell density in niches across several tumor types in an earlier study, points out that CD8⁺ – together with several other T-cell subsets – orchestrate general T-cell niches (Blessin et al., 2021b).

3. The relative intensity of the immune checkpoint receptors CD112R and PD-1 was calculated by dividing the raw intensity values by the corresponding reference cells (i.e., a CD112R over-expressing HeLa reference cell line for CD112R and the follicular T-helper cells in healthy normal reference tonsils).

A



B



C

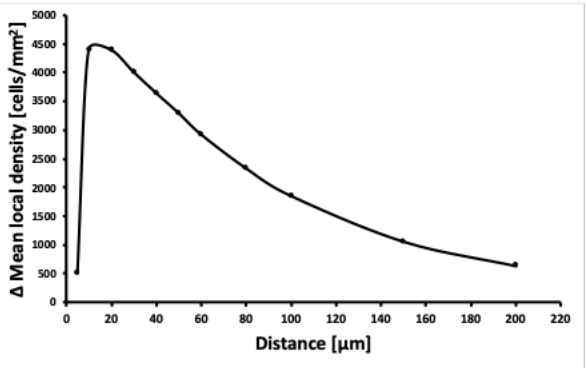


Figure 4: Automated T-cell niche detection by the combination of local density measurements and a deep learning-based cell detection. The highest accuracy of T-cell niche detection was achieved by calculating the local density of index cells at a 20 μ m radius. For this purpose, 20 annotations of niche and non-niche were made by a pathologist.

2.6.2 TMA analysis

For TMA analysis, spots were manually segmented using the Visiopharm software package (Hoersholm, Denmark). Five parameters were measured for every TMA core or tissue compartment:

1. The density of each measured immune cell phenotype per square millimeter was calculated by dividing the number of the immune cells by the measured area of each tissue spot. The tissue area was measured by a DeepLab3⁺ deep learning algorithm, which we have trained on 150 TMA spots using python version 3.8 (Foundation, 2021) and the Visiopharm software package (Hoersholm, Denmark).
2. The percentage of each immune cell subtype was calculated by dividing the number of positive cells of this specific subset (e.g., CD8⁺Ki67⁺) by the total number of cells belonging to the same distinct phenotype (e.g., CD8⁺) (Blessin et al., 2021c).
3. The relative intensity of the immune checkpoint receptors CD112R and PD-1 was calculated by dividing the raw intensity values by the corresponding reference cells (Blessin et al., 2019).
4. The fraction of immune cells located in a T-cell niche which was identified as described below.

2.7 Statistical analysis.

JMP Pro 14 software package (SAS Institute Inc., NC, USA) and R version 3.6.1 (The R foundation) (Tippmann, 2015, R-Core-Team, 2021) were used in this study. The clinico-histopathological parameters of the patients were reported as counts and percentages for categorical data. To study the relationship between immune cell densities and clinicopathological parameters, contingency table analysis and likelihood ratio Chi-square test were used. The prognostic value of immune checkpoint expression and other CD8⁺ cytotoxic T-cell parameters, Kaplan-Meier Estimates (R “survival” (Therneau and Grambsch, 2000) package) were used for overall survival as the study endpoint. The log-rank test was applied to assess differences between groups in Kaplan-Meier Estimates. Continuous parameters were allocated to groups for survival analysis according to the average. Time-dependent areas under receiver operating characteristic curves were used to estimate the predictive performance of immune environment scores (R “riskRegression” (Blanche et al., 2013) package). All p-values were two-sided, and p-values <0.05 were considered as significant.

The “Rtsne” package was used to perform the t-distributed stochastic neighbor embedding (t-SNE) algorithm. The per cell data retrieved from our cell detection deep learning algorithm were normalized by log-transformation (Kobak and Berens, 2019) and used as input for the t-

SNE algorithm. The perplexity, theta, and iteration parameters were selected by systematic visual inspection to illustrate patterns of CD112R and PD1 expression on proliferating and non-proliferating CD8⁺ cytotoxic T-cells. Unsupervised cluster analysis using custom R scripts based on “gplots, hclust” was applied on the per cell as well as the mean per patient densities/intensities of the stained markers (Samusik et al., 2016). For unsupervised cluster analysis, the densities and intensities were normalized using the Min-max algorithm (Cao et al., 2016). The colors in the heat map represent the normalized measurements of a given cluster.

3. Results

3.1 Expression profile of CD112R and PD-1 on CD8⁺ T-cells

A total of 20 (100%) colorectal cancer large sections and 503 (96%) of 522 colorectal cancer patients in one tissue microarray (TMA) format were interpretable in this study. The remaining 19 tumor samples were excluded due to missing tissue, a non-representative small number of cells (<200 cells), or blurry tissue. A total of 257'767 (2.5%) CD8⁺ T-cells of 10'471'289 cells were analyzed (TMA: 18584 (1.7%) CD8⁺ T-cells of 1'124'462, Large sections: 239233 (2.6%) CD8⁺ T-cells of 9'346'827). Both immune checkpoints were detected on CD8⁺ T-cells (Figure 5). Regardless of the localization, CD112R was expressed by a majority (57%) of CD8⁺ cytotoxic T-cells, while PD-1 expression was only found on a smaller subset (29%) of CD8⁺ T-cells (Figure 4-5). Although co-expression of both immune checkpoint receptors was seen on 19% of all CD8⁺ T-lymphocytes, a high expression of both immune checkpoints was detected in less than 1% of CD8⁺ T-cells. Despite the fact that joint occurrence of high CD112R and high PD-1 expression did also not exceed 1% in different tissue compartments (e.g., niche, non-niche, invasive margin, center of the tumor), the fraction of CD8⁺ T-cells expressing immune checkpoints was higher in niche (75%) compared to non-niche (65%) tissue compartments.

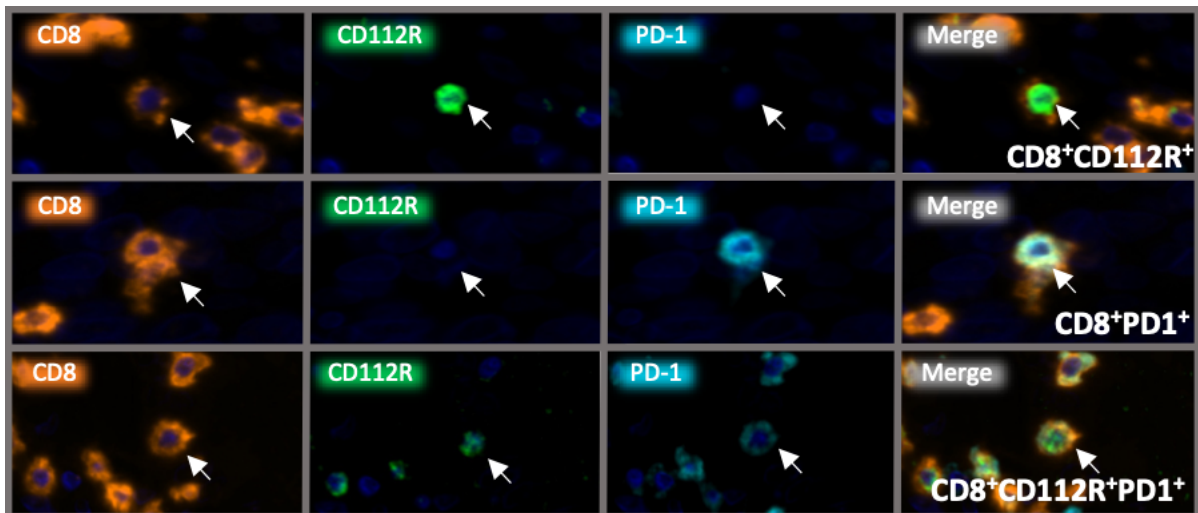


Figure 5: Representative CD8⁺ cytotoxic T-cell with high CD112R expression (top), high PD-1 expression (middle), and typical low expression of both immune checkpoints are displayed. (184x magnification)

3.2 T-cell niche detection

3.2.1 T-cell-niche detection in large section

Before quantifying T-cell niche, the overall CD8⁺ T-cell density of each large section in the center of tumor and at the invasive margin was evaluated. The CD8⁺ T-cell density at the

invasive margin was significantly higher than in the center of tumor ($p=0.0024$). The mean $CD8^+$ T-cell density at the invasive margin was 489 ± 335 cell/ mm^2 (rang from 131 to 1595 cell/ mm^2). The mean $CD8^+$ T-cell density in the center of tumor was 180 ± 260 cell/ mm^2 (rang from 181 to 1093 cell/ mm^2). The heatmap, based on a deep learning cell detection, was used to visualize the data and anticipate T-cell niche location compared with the T-cell-detection algorithm (Figure 6).

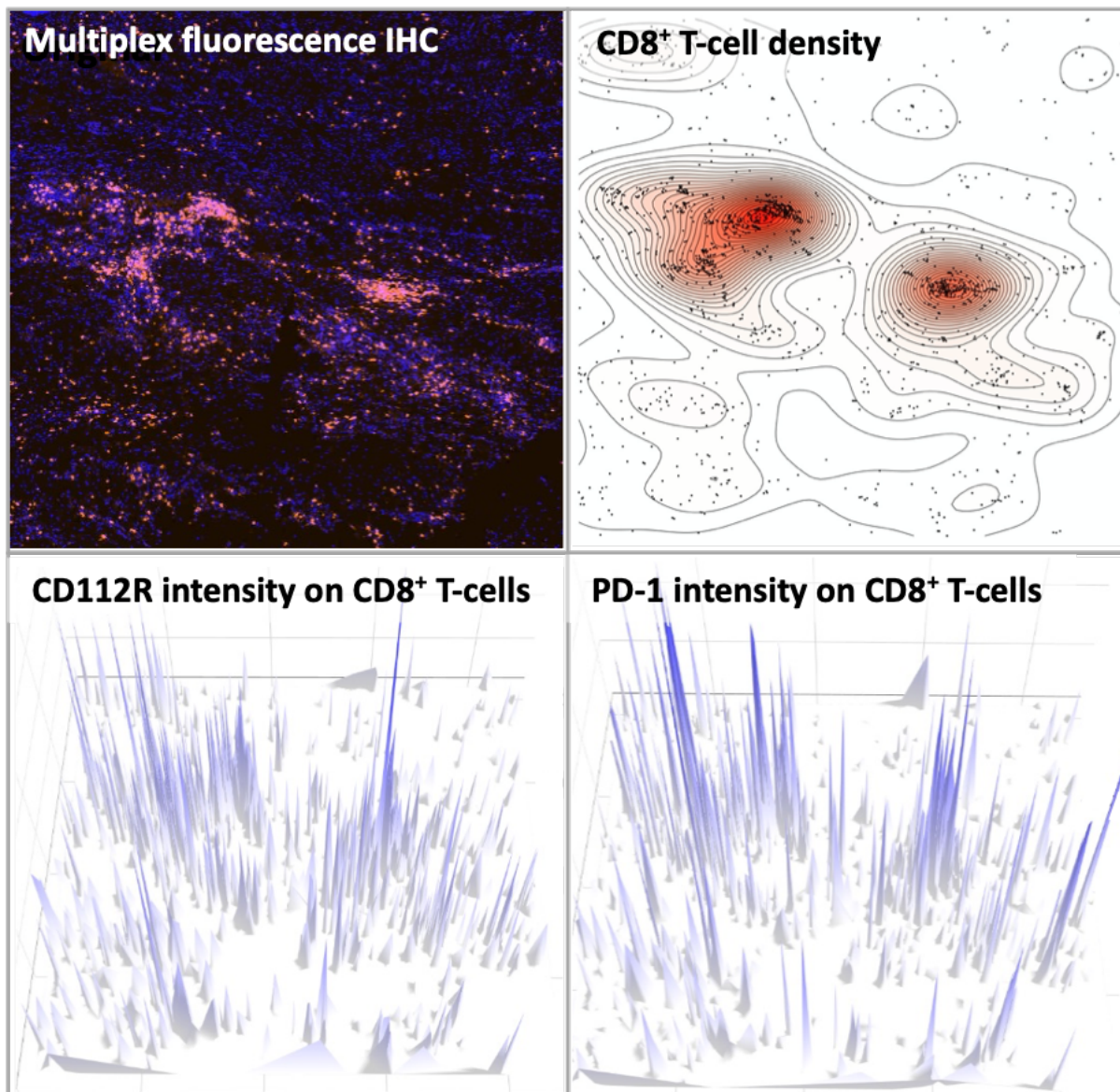


Figure 6: The raw mflHC image and density heatmaps ($CD8^+$ T-cell density (red), CD112R relative intensity on $CD8^+$ T-cells (blue), and PD-1 relative intensity on $CD8^+$ T-cells (blue)) are shown.

To further quantify the T-cell niche, we performed the T-cell niche detection algorithm on 20 large sections. The heatmap visualization based on the T-cell niche detection algorithm was shown in the following plot (Figure 7). In 20 large sections, the fraction of $CD8^+$ T-cells expressing immune checkpoints in niche was higher than non-niche compartments. 29892

(41.6%) CD112R⁺CD8⁺ T-cells and 24832 (34.6%) PD-1⁺CD8⁺ T-cells were located in T-cell-nests.

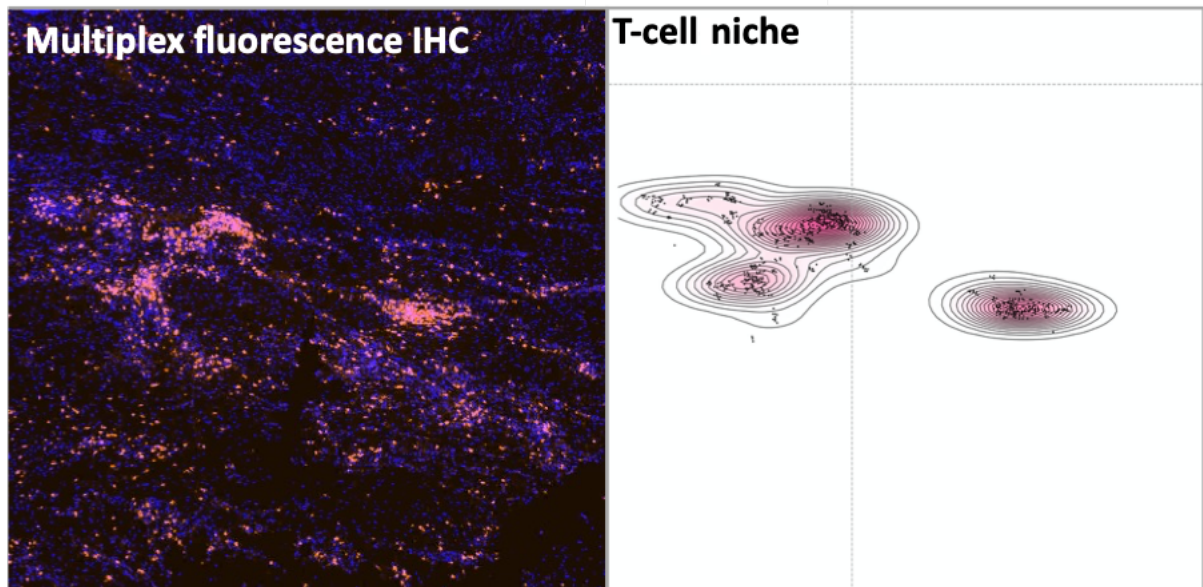


Figure 7: The raw multiplex fluorescence IHC image (left) and the heatmap visualization of automated T-cell niche detection (right) are shown.

3.2.1 T-cell niche detection in TMA

T-cell niche detection was also applied on a TMA. To clarify the expression levels of CD112R and PD-1 on CD8⁺ T-cells in T-cell niches, a t-SNE algorithm was performed in the TMA study cohort (Figure 8). The immune checkpoints (CD112R and PD-1) were detected on both niche and non-niche compartments. 4911 (26.5%) of 18584 of the CD8⁺ T-cells were orchestrated in T-cell niches. The fraction of CD8⁺ T-cells expressing immune checkpoints in niche was higher than non-niche compartments. 3335 (67.9%) CD112R+CD8⁺ T-cells were detected in niche. 1592 (32.4%) PD-1+CD8⁺ T-cells were detected in niche. 7267 (53.1%) CD112R+CD8⁺ T-cells were detected in non-niche. 3792(27.7%) PD-1+CD8⁺ T-cells were detected in non-niche.

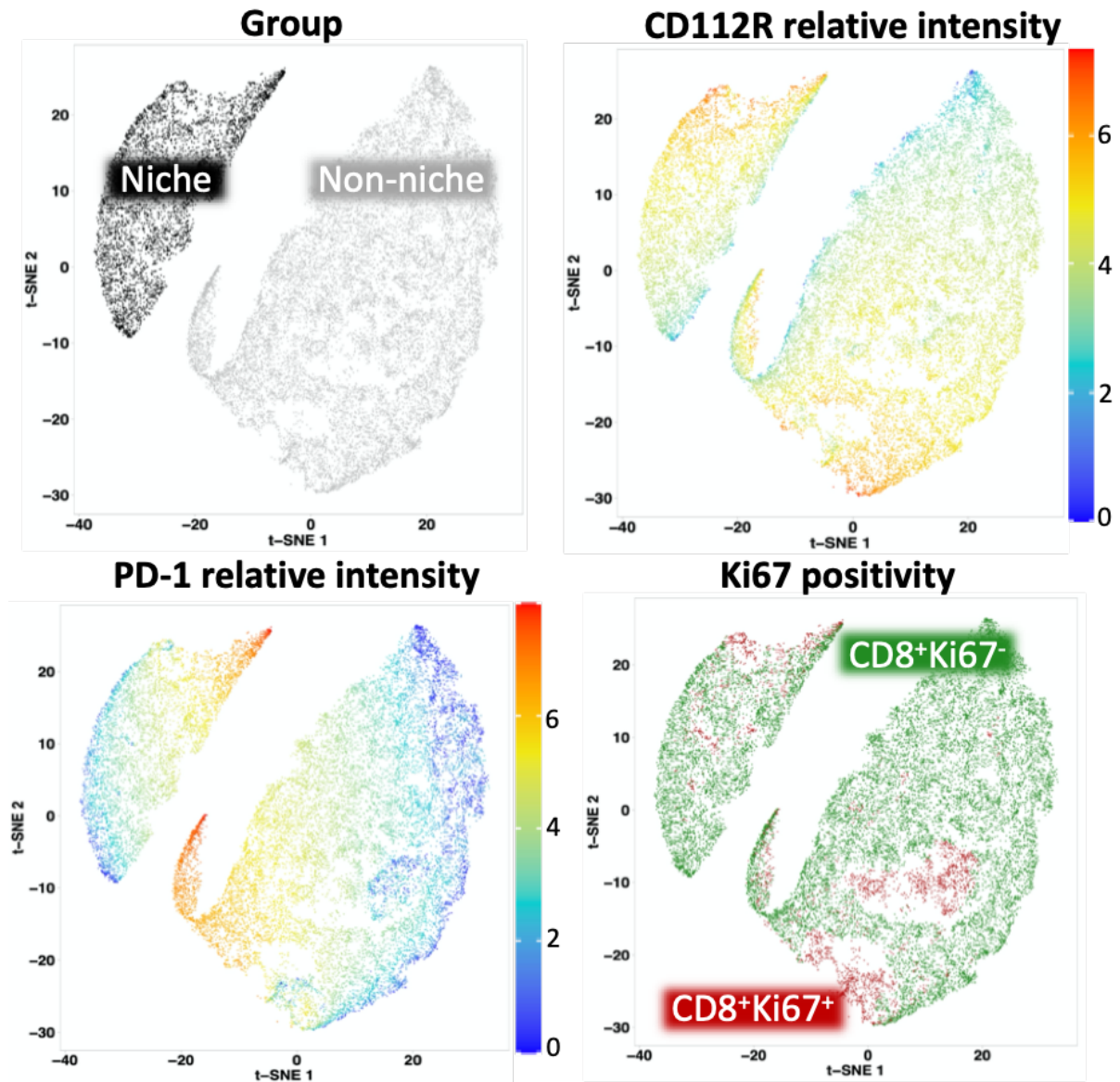


Figure 8: The expression level of CD112R, PD-1, and Ki67 on the CD8⁺ T-cells located in T-cell niches and other tissue compartments (non-niche) are shown according to the t-distributed stochastic neighbor embedding (t-SNE) algorithm. Each point represents a single CD8⁺ T-cell sample, and the axes (t-SNE1 and t-SNE2) have arbitrary units. The more similar the samples are, the closer together they appear on the t-SNE plot.

3.3 Upregulation of CD112R and PD-1 on CD8⁺ T-cells in T-cell niche

3.3.1 Quantifying CD112R and PD-1 expression on CD8⁺ T-cells in compartments

To study the localization depending expression profile of CD112R and PD-1 on CD8⁺ cytotoxic T-cells, an automated algorithm for T-cell niche detection was applied. Across 20 colorectal cancer large sections, local enrichments of the CD8⁺ T-cell density were found and identified as T-cell niches. Representative inflamed and non-inflamed cases (including center of tumor and invasive margin) were accordingly displayed, showing the raw IHC image, T-cell location,

CD8 density, CD112R relative intensity on CD8⁺ T-cells, and PD-1 relative intensity on CD8⁺ T-cells (Figure 9, Figure 10).

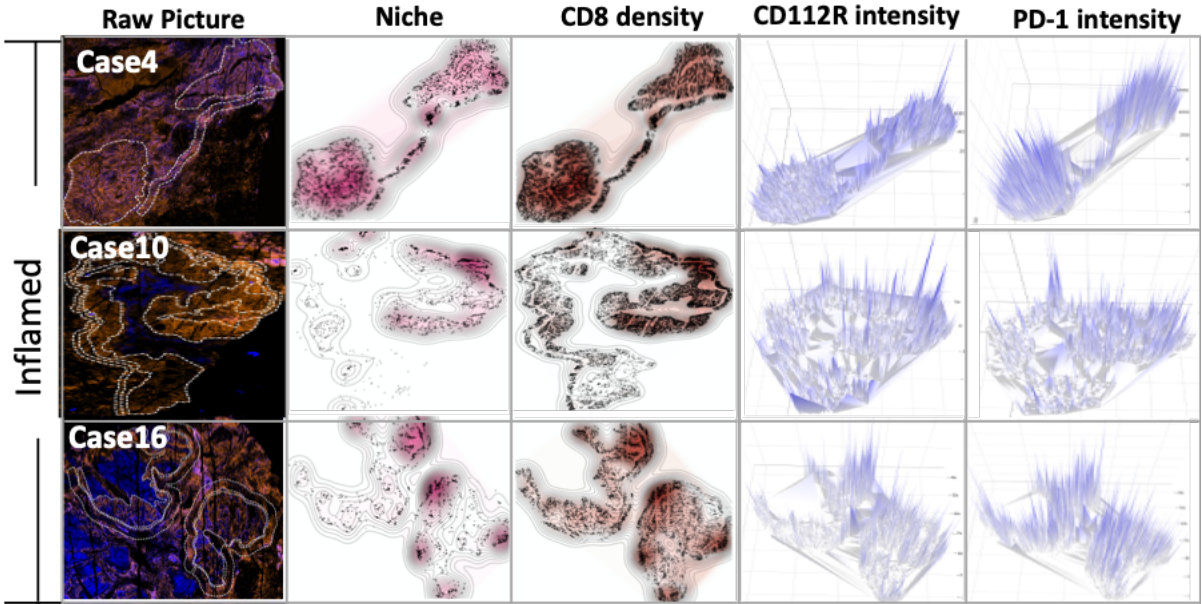


Figure 9: Density heatmaps showing the automated T-cell niche detection (pink), CD8⁺ T-cell density (red), and CD112R and PD-1 relative intensity (blue) for 3 cases with an inflamed immune phenotype.

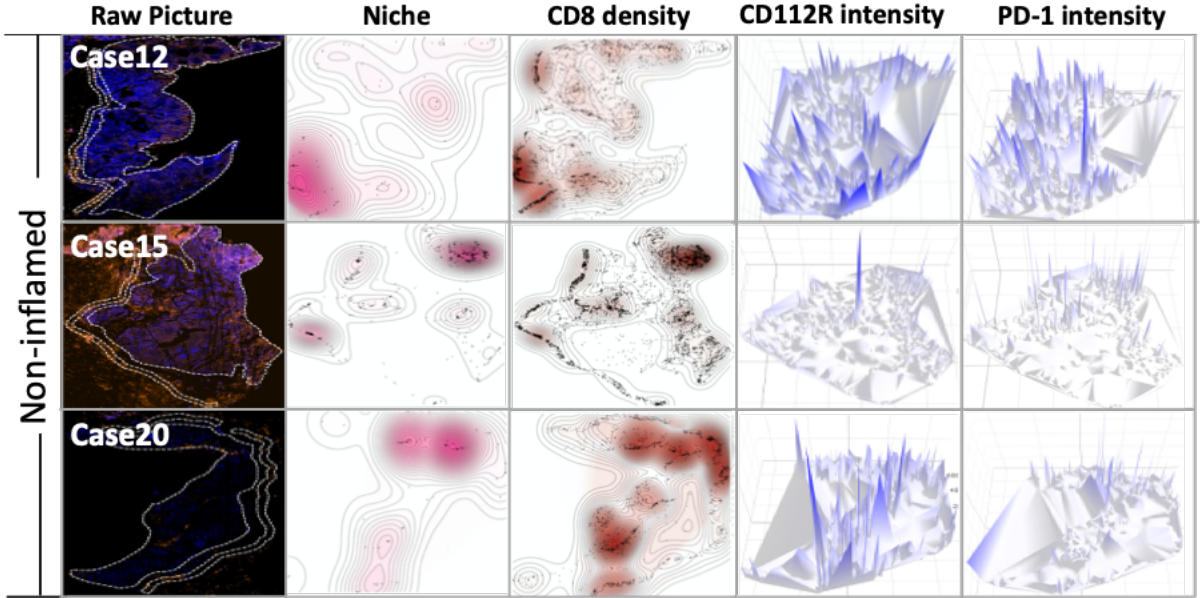


Figure 10: Density heatmaps showing the automated T-cell niche detection (pink), CD8⁺ T-cell density (red), and CD112R and PD-1 relative intensity (blue) for 3 cases with a non-inflamed phenotype (bottom).

3.3.2 Unsupervised cluster analysis of large section

Unsupervised cluster analysis of large section included CD8⁺ T-cells density, CD112R and PD-1 relative intensity on CD8⁺ T-cells as well as proliferating rate of CD8⁺ T-cells across niche and non-niche compartments. Unsupervised cluster analysis of these parameters revealed two major clusters, which met the criteria of an immune inflamed and immune desert phenotype (Figure 11). Hence, the fraction of CD8⁺ T-cell in niche was higher in the inflamed immune phenotype. Interestingly, the CD112R and PD-1 expression level was upregulated on CD8⁺ cytotoxic T-cells in an inflamed immune phenotype and on CD8⁺ T-cells located in T-cell niches (each p<0.001, Table 4). However, the CD112R expression level was significantly higher in CD8⁺ T-cells located at the invasive margin while PD-1 was upregulated in the center of the tumor (each p<0.001, Table 4).

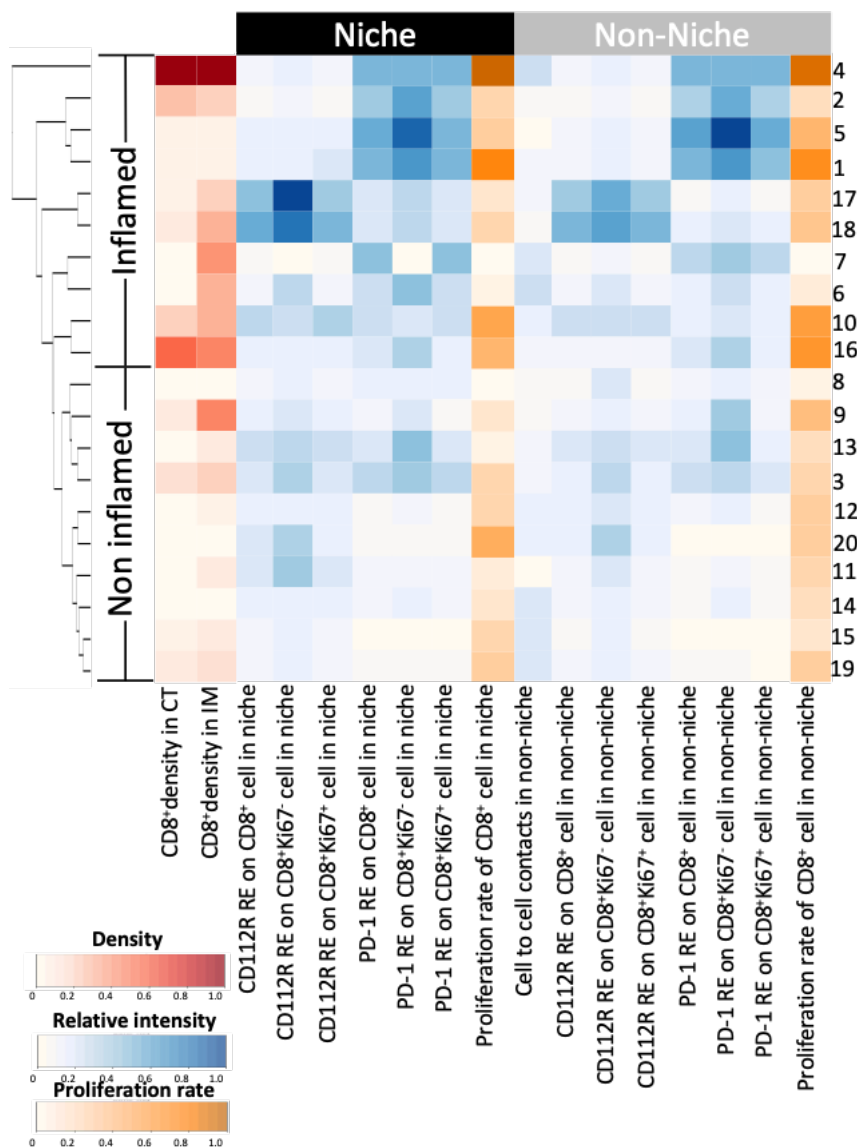


Figure 11: An unsupervised cluster analysis of the CD8⁺ T-cell density (red), cell-to-cell contacts (green), CD112R and PD-1 relative intensity (RE, blue) and proliferation rate of CD8⁺ T-cells identified cases with an inflamed (top) as well as with a non-inflamed immune phenotype is depicted.

Compartments	Patient number	CD112R relative intensity	p-value	PD-1 relative intensity	p-value
Niche vs. Non-niche			<0.001		<0.001
Niche	20	0.92 (\pm 1.17)		0.79 (\pm 0.87)	
Non-niche	20	0.81 (\pm 1.04)		0.66 (\pm 0.86)	
Immune phenotypes			<0.001		<0.001
Inflamed	10	0.92 (\pm 1.23)		0.86 (\pm 0.94)	
Non-inflamed	10	0.67 (\pm 0.65)		0.37 (\pm 0.54)	
Tissue compartments			<0.001		<0.001
Center of tumor	20	0.74 (\pm 0.93)		0.81 (\pm 0.93)	
Invasive margin	20	1.05 (\pm 1.33)		0.46 (\pm 0.63)	

Table 4: Association between relative CD112R and PD-1 expression level and the localization of the CD8⁺ T-cells.

3.4 CD112R and PD-1 upregulation on CD8⁺Ki67⁺ T-cells in tissue compartments and immune phenotypes

3.4.1 The proliferating and non-proliferating CD8⁺ T-cell subsets

The two main subsets of CD8⁺ T-cells (proliferating CD8⁺ T-cells and non-proliferating CD8⁺ T-cells) and corresponding immune checkpoints (CD112R and PD-1) expression were analyzed in this study (Figure 12,13). CD112R and/or PD-1 expression was detected on both the proliferating (Ki67⁺) as well as the non-proliferating CD8⁺ T-cell subset. The distribution of CD112R relative intensity and PD-1 relative intensity on the proliferating and non-proliferating subsets was shown using t-SNE algorithm (Figure 12).

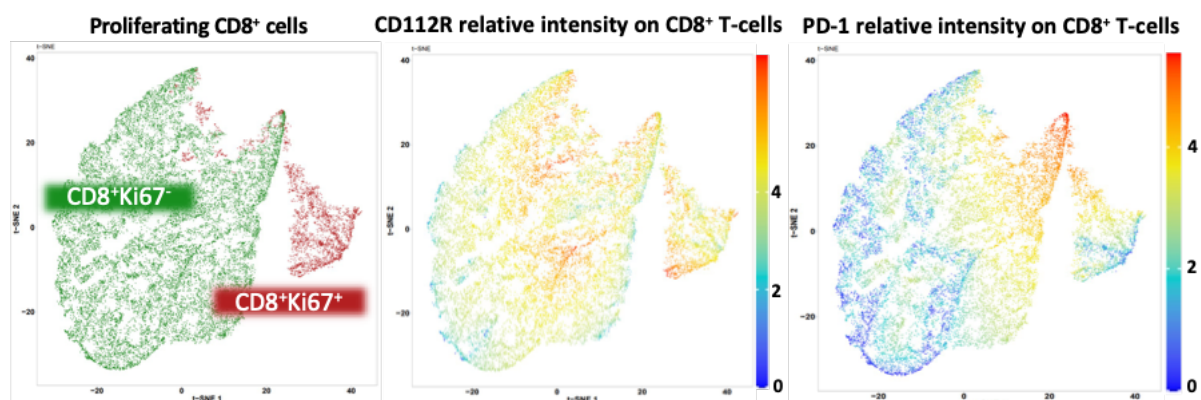


Figure 12: The expression level of CD112R and PD-1 on the proliferating CD8⁺ T-cells and non-proliferating CD8⁺ T-cells is shown according to the t-SNE algorithm. Each point represents a single CD8⁺ T-cell sample, and the axes (t-SNE1 and t-SNE2) have arbitrary units. The more similar the samples are, the closer together they appear on the t-SNE plot.

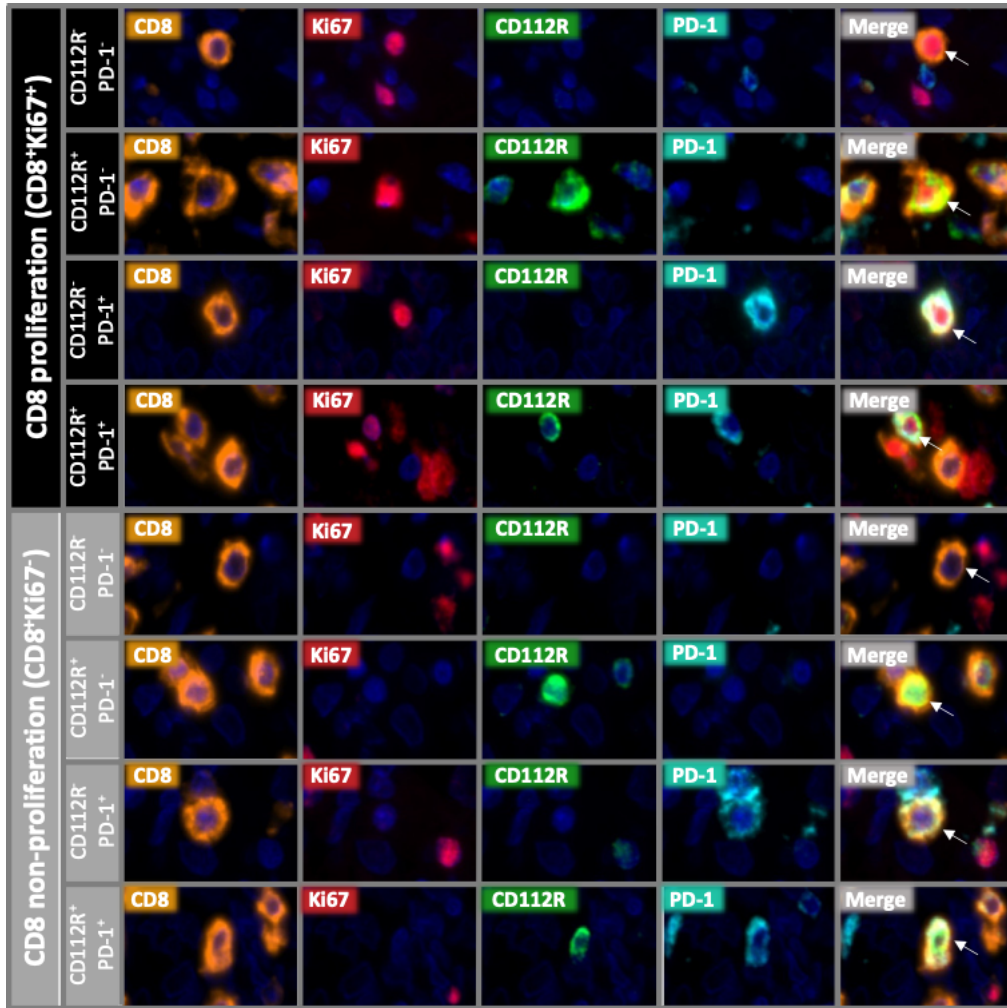


Figure 13: Representative multiplex fluorescence immunohistochemistry images of proliferating CD8⁺ T-cells and non-proliferating CD8⁺ T-cells in colorectal cancer. The expression of CD8 (orange), Ki67 (red), CD112R (green), and PD-1 (blue) are individually displayed. (184x magnification)

3.4.2 Significant upregulation of Immune checkpoints in CD8⁺Ki67⁺ subset.

Highest expression levels of both immune checkpoints were commonly also not found co-expressed in proliferating as well as non-proliferating CD8⁺ cytotoxic T-cells. Although the proliferation rate of CD8⁺ T-cells was not significantly ($p=0.5$) different between the T-cell niches and other Tissue areas, the CD112R and PD-1 expression was significantly higher in the proliferating compared to the non-proliferating CD8⁺ T-cell subset across all analyzed tissue compartments and immune phenotypes ($p<0.001$ each, Figure 14-15). The highest immune checkpoint upregulation of the proliferating compared to the non-proliferating subset was identified at the invasive margin (1.5-fold) for CD112R and in the non-inflamed immune phenotype for PD-1 (2.3-fold, Figure 14-15). The lowest difference in the expression level between both CD8⁺ cell subsets was seen in T-cell niches for CD112R (1.1-fold) and PD-1 (1.4-fold, Figure 14-15).

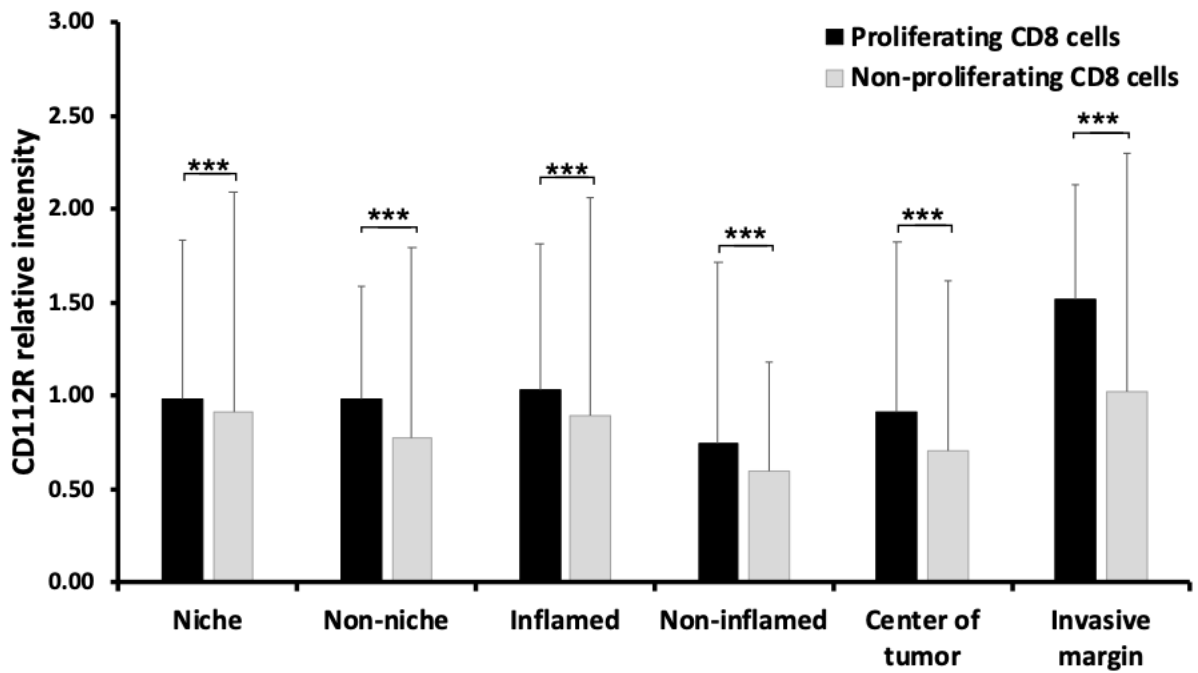


Figure 14: The relative intensity of CD112R is shown significantly increased (** $p < 0.001$) on the proliferating (black) compared to the non-proliferating (grey) CD8⁺ T-cell subset.

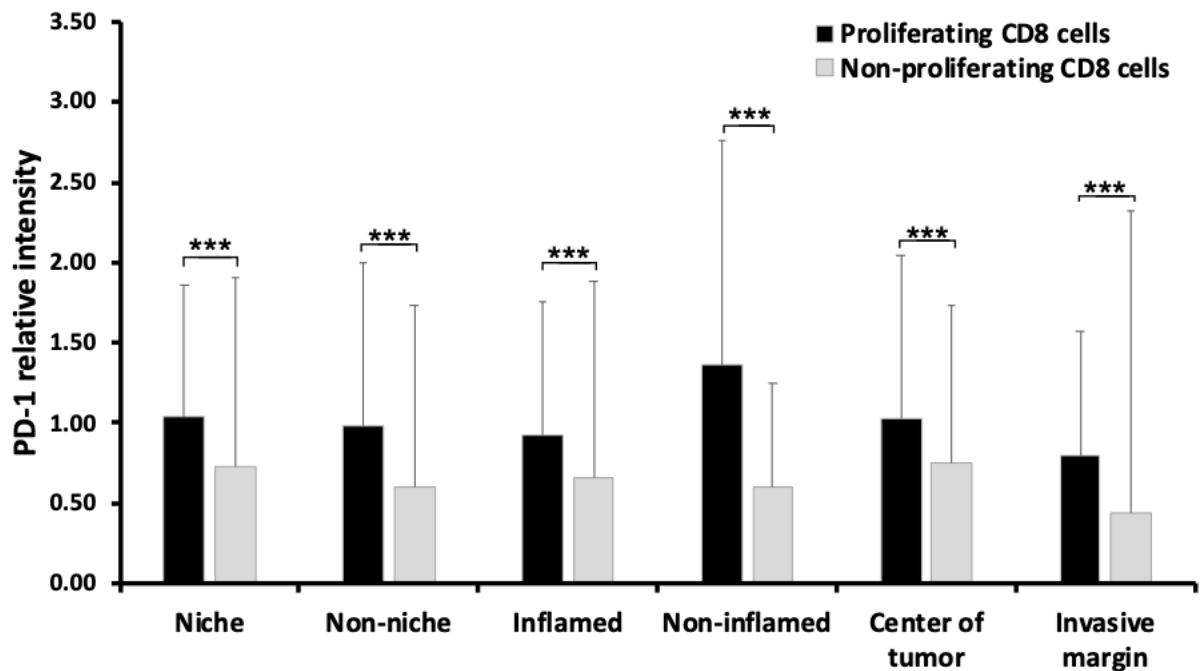


Figure 15: The relative intensity of PD-1 is shown significantly increased (** $p < 0.001$) on the proliferating (black) compared to the non-proliferating (grey) CD8⁺ T-cell subset.

3.5 Prognostic relevance of spatial niche information

To address the question of whether the spatial orchestration in niches of CD8⁺ T-cell subsets had a greater role in the tumor microenvironment compared to the widely used density of tumor-infiltrating lymphocytes, the density of T-cell subsets, the relative intensity of CD112R and PD-1, the proliferation rate of CD8⁺ T-cells, and the localization in T-cell niche were linked to clinicopathological data as well as overall survival. Elevation of all these parameters – representing an inflamed tumor microenvironment – were linked to a prolonged overall survival in univariate analysis (Table 5). In univariate analysis, the fraction of CD8⁺ T-cells located in T-cell niches (HR: 1.58, p=0.006) and the CD112R relative intensity on CD8⁺ T-cells (HR: 1.56, p<0.001) showed a higher hazard ratio compared to the CD8⁺ T-cell density (HR:1.34, p=0.028, Table 5).

	Fraction of CD8 ⁺ T-cells in niche	CD112R relative intensity on CD8 ⁺ T-cells	PD-1 relative intensity on CD8 ⁺ T-cells	CD8 ⁺ T-cell density	Fraction of proliferating CD8 ⁺ T-cell
HR:	1.58 (1.14-2.19)	1.56 (1.25-1.94)	1.46 (1.17-1.82)	1.34 (1.03-1.75)	1.19 (0.92-1.53)
p-value	0.006	<0.001	<0.001	0.028	0.19

Table 5: Univariate analysis of fraction of CD8⁺ T-cells in niche, CD112R relative intensity on CD8⁺ T-cells, PD-1 relative intensity on CD8⁺ T-cells, CD8⁺ T-cell density, and fraction of proliferating CD8⁺ T-cells is shown.

3.5.1 Unsupervised cluster analysis of TMA

Unsupervised cluster analysis of TMA includes the fraction of CD8⁺ T-cells, CD8⁺ T-cells density, and immune checkpoints (CD112R and PD-1) relative intensity on CD8⁺ T-cells (Figure 16). Based on the dendrogram of unsupervised cluster, TMA patients are further divided into two clusters (a and b cluster and four clusters (a1, a2, b1, and b2), the corresponding survival analysis demonstrated significant (p<0.001 each) prognostic relevance (Figure 17).

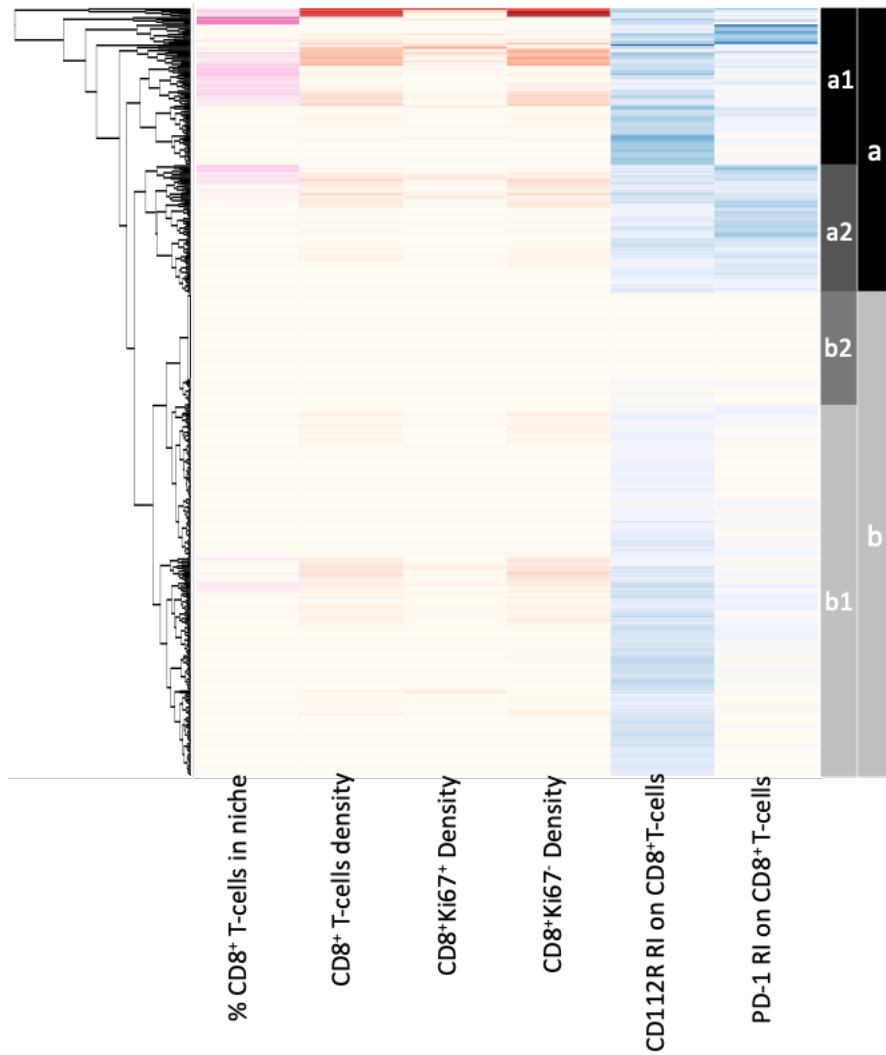


Figure 16: An unsupervised cluster analysis of the fraction of CD8⁺ T-cells in niche (pink), CD8⁺ T-cells density (red), CD8⁺Ki67⁺ density (red), CD8⁺Ki67⁻ density (red), CD112R relative intensity on CD8⁺ T-cells (blue), and PD-1 relative intensity (blue) on CD8⁺ T-cells is depicted.

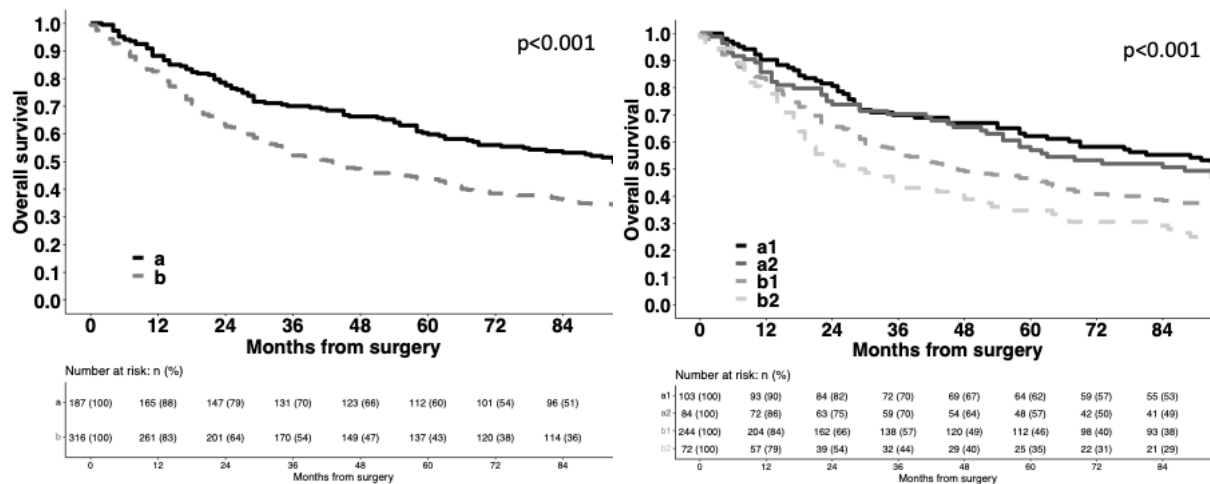


Figure 17: The Kaplan-Meier Estimates analysis based on the unsupervised cluster (two clusters: **a** and **b** and four clusters: **a1**, **a2**, **b1**, and **b2**) is displayed.

3.5.2 Time-dependent receiver operating characteristic analysis

ROC curves revealed that the niche integrated phenotypes from all available spatial and immune checkpoint expression parameters in unsupervised cluster analysis (AUC: 0.65, 0.60-0.70) had significantly ($p < 0.001$) higher prognostic performance than the CD8⁺ T-cell density phenotypes from the survival analysis based on an unsupervised cluster analysis of T-cell densities (AUC: 0.57, 0.53-0.61) (Figure 18).

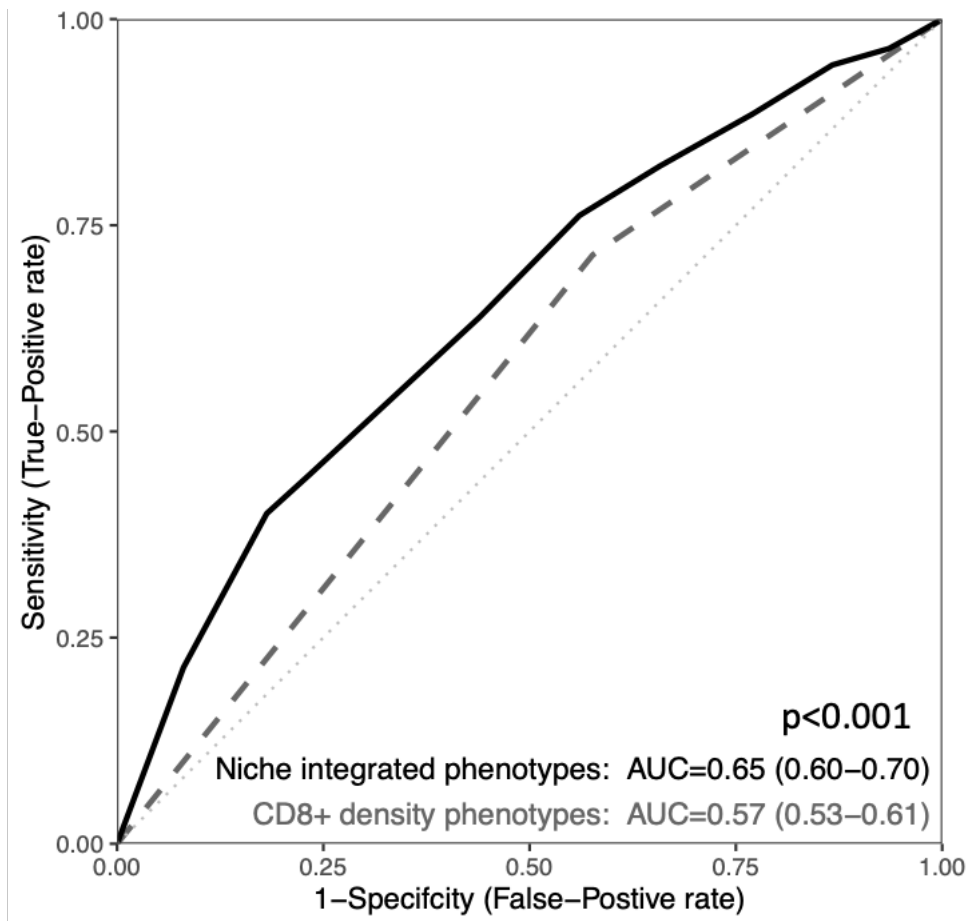


Figure 18: Time-dependent receiver operating characteristic curve with niche integrated phenotypes (black) and CD8⁺ T-cell density phenotypes (grey) is displayed.

4. Discussion

This purpose of this study was to assess the expression level and spatial orchestration of CD112R and PD-1 on proliferating (Ki67+) as well as non-proliferating (Ki67-) CD8⁺ T-cells in a historical cohort of 523 colorectal cancers. Thus, the spatial organization of CD8⁺ T-cells was evaluated in several tissue compartments and the relative immune checkpoint expression was evaluated on cytotoxic T-cells.

The role of tumor infiltrating lymphocytes, to predict patients' outcome (Galon et al., 2006) and response to immune checkpoint therapy (Havel et al., 2019), has been studied extensively in colorectal cancer, while only little is known about the spatial distribution patterns of TILs in the tumor microenvironment and its impact on patients' survival. This might be due to the inconsistent definitions of TILs accumulations across several solid tumor types and the technological hurdle in automated assessment: In colorectal cancer, dense T-cell accumulations in the tumor microenvironment were identified as tumor-associated lymphoid nodules which are similar to normal lymphoid nodules but often be detected in the tumor region (McMullen et al., 2010), tertiary lymphoid tissue which is an ectopic lymphoid tissue and involve in the adaptive immune response (Di Caro et al., 2014), and ectopic lymphoid-like structures (Pitzalis et al., 2014) via manual inspection using H&E and conventional brightfield immunohistochemistry (e.g., lymphocyte markers, professional antigen presenting immune cell markers). In other tumor entities, accumulations of TILs were characterized as lymphocyte clusters, which refers to the area where B-cells are enriched. These characterizations were set using manual identification in multiplex fluorescence IHC as well as gene expression profiling in malignant melanoma (Cabrita et al., 2020) and as intratumoral APC niches (stem-like CD8⁺ T-cells reside in APC niche) by manual annotation of multiplex fluorescence IHC staining in several solid cancer types such as kidney cancer, prostate cancer, and bladder cancer (Jansen et al., 2019). To address this issue, a framework for automated T-cell niche detection, which comprises a deep learning step for cell detection and an algorithm for detecting the local TILs density adjacent to the index cell – using multiplex fluorescence immunohistochemistry staining – was developed and validated in this study. The accuracy of the new approach for appropriate T-cell niche identification was validated by the concordance of the data with previous manual studies (McMullen et al., 2010, Di Caro et al., 2014) and the striking prognostic impact of cytotoxic T-cells located in T-cell niches.

In colorectal cancer, 57% of CD8⁺ T-cells showed a CD112R expression, which was consistent with Whelan et al.: 60-80% of CD8⁺ T-cells expressed CD112R in a variety of tumor entities (e.g., ovarian cancer, renal cancer, colon cancer) (Whelan et al., 2019). The data also showed that 29% of CD8⁺ T-cell co-expressed CD112R and PD-1, compared with 44% of CD8⁺ T-cells

co-expressing CD112R and PD-1 in flow cytometry analysis (Whelan et al., 2019). However, the high expression of both immune checkpoints was detected in less than 1% of CD8⁺ T-cells. In an earlier study, delayed transcription and protein expression of CD112R were observed compared to TIGIT, which indicates the low co-expression of high CD112R and PD-1 may be due to the fact that CD112R and PD-1 may not be expressed at the same phase of T-cell exhaustion (Murter et al., 2019). Overall, the efficiency of automated quantification of CD112R and PD-1 expression on CD8⁺ T-cells was validated by the concordance of our data with previous studies.

The data from this study identified upregulation of CD112R and PD-1 on proliferating CD8⁺ cytotoxic T-cells irrespective of the tissue compartment (i.e., niche, non-niche, inflamed, non-inflamed, center of tumor, invasive margin). These findings were in line with previous studies showing that the increased PD-1 and CTLA-4 expression on proliferating CD8⁺ T-cells (Kamphorst et al., 2017) and a high PD-1 expression level was observed on proliferating (Ki67⁺) CD11a⁺ CD8⁺ cytotoxic T-cells (Liu et al., 2013). Interestingly, CD112R and PD-1 represent exhaustion of T-cells (Zhu et al., 2016), whereas Ki67 indicates proliferation of T-cells (Cuylen et al., 2016). Although proliferating CD8⁺ T-cells are showing hallmarks of exhaustion by expressing CD112R and PD-1, there is evidence that it might preserve its effector function. Kamphorst et al., found that a high fraction of inhibitory immune checkpoint receptors (PD-1) on proliferating CD8⁺ T-cell were linked to tumor regression after anti-PD-1 therapy (Kamphorst et al., 2017). Moreover, a particular subset of PD-1⁺CD8⁺ was recognized as stem-like T-cell with proliferative capacity (Utzschneider et al., 2016). Taken together, it is tempting to speculate that proliferating CD8⁺ T-cells might retain ability to control tumor growth along with the expression of several exhaustion biomarkers.

The fact that both inhibitory immune checkpoint receptors (i.e., CD112R and PD-1) were upregulated on cytotoxic T-lymphocytes located in T-cell niches compared to all other tumor components suggest an influence of the location in the tumor microenvironment on the cytotoxic T-cell effector/ exhaustion state. In agreement with our result, several earlier publications have shown that the upregulation of inhibitory immune checkpoint receptors occurs during constant T-cell stimulation in various conditions. For example, in chronic virus infection and cancer environment, the inhibitory immune checkpoint expression was increased due to sustained stimulation (McLane et al., 2019). The high PD-1 and TIGIT expression were observed in tumor-infiltrating lymphocytes in a study using flow cytometry (Hung et al., 2018). High PD-1 expression was detected in Melan-A melanoma (MLANA) antigen-specific CD8⁺ T-cells compared with normal tissue (Ahmadzadeh et al., 2009). Elevated PD-1 expression was observed with RNA sequencing during the therapy with checkpoint inhibitors (Riaz et al., 2017).

However, growing evidence indicates that high expression levels of inhibitory immune checkpoint receptors does not necessarily indicate irreversible T-cell dysfunction. For instance, there are several distinct T-cell subsets showing an exhausted phenotype along with preserved effector function or anti-cancer reactivity such as precursors of exhausted T-cells (TPEX): TCF1⁺ cells which maintain high effector function, regeneration, and differentiation ability (Utzschneider et al., 2020, Siddiqui et al., 2019). Furthermore, follicular T-helper cells which express PD-1 are capable of accumulating T-cells to the germinal center and regulating the follicular recruitment (Shi et al., 2018). Moreover, PD-1^T lymphocytes (distinct intertumoral CD8⁺ T-cell population with high PD-1 expression levels) display a strikingly different transcriptional and metabolic landscape other than CD8⁺ T-cells expressing low/negative PD-1 and exhibit a strong prognosis relevance (Thommen et al., 2018). Interestingly, there is evidence that the PD-1^T lymphocytes are largely localized in the tertiary lymphoid structures and significantly produce CXCL13 which mediates immune cell recruitment to T-cell niches (Thommen et al., 2018). This fact is a strong evidence for incorporating the location of cytotoxic T-cells as one parameter of T-cell function together with other effector and exhaustion markers as well as gene signatures to fully characterize the state of T-cell activation.

The observation that a comprehensive assessment of the immune tumor microenvironment – by taking T-cell niches, immune checkpoint expression levels, and CD8⁺ T-cell subset densities into account – showed a significantly better predictive performance for patients' overall survival compared to the sole analysis of T-cell densities, underlines the importance of T-cell localization for patients' outcome. In agreement with these results, a favorable prognostic relevance has been described for some of the analyzed immune components in individual earlier studies. For example, a high CD8⁺ T-cell density in the invasive margin and the center of tumor (Galon et al., 2006, Blessin et al., 2021c), a high proliferation rate of CD8⁺ cytotoxic T-cells (Blessin et al., 2021c), an elevated PD-1 expression levels (Berntsson et al., 2018), a high CD112R gene expression (Tang et al., 2019), and a high number of T-cells orchestrated in T-cell accumulations (McMullen et al., 2010, Di Caro et al., 2014) were associated with a favorable prognosis in colorectal cancer. This corresponds to the fact that the quantity of T-cells represents only one out of a multitude of hallmarks characterizing the individual immune phenotypes (e.g., immune inflamed, immune excluded and immune desert phenotype) (Chen and Mellman, 2017). Therefore, these data emphasize to also incorporate the T-cell niche compartment in scores for patient's outcome rather than just quantifying the T-cell density of the whole tumor center or the invasive margin.

Although CD112R and PD-1 were both elevated in T-cell niches, a co-expression at low expression levels was only found in around 20% of all CD8⁺ cytotoxic T-cells, co-expression

at high levels was virtually absent, and CD112R was downregulated – while PD-1 was upregulated – in the center of the tumor. Thus, the histomorphological and phenotypical differences between both inhibitory immune checkpoints presented in this study emphasize a non-redundant function of both molecules in the tumor microenvironment and indicate CD112R and PD-1 as putative targets for a dual immune checkpoint receptor blockade. Accordingly, several unique aspects of CD112R were identified: Such as a significant association with an Eomes⁺T-bet⁻ expression, which indicated the state of T-cells exhaustion and the rapid internalization of CD112R which might be correlated with regulatory mechanisms of CD112R (Whelan et al., 2019). Moreover, *in vitro* T-cell functional assays revealed that dual blockade of CD112R and PD-1 lead to a synergistic and additive effect on the IFN γ production and thus to enhance CD8⁺ T-cell cytokine production and effector function compared to the sole use of one immune checkpoint inhibitor (Whelan et al., 2019). This might be explained by a non-redundant lymphocyte inhibitory pathway of both immune checkpoint receptors. While PD-1 mediates its inhibitory function via the tyrosine phosphatase SHP-2 that leads to reduced phosphorylation of molecules within the T-cell receptor signaling cascade (Keir et al., 2008), there is some evidence that CD112R is rather in an interplay with SHIP than SHP-2 (Zhu et al., 2016). Zhu et al., found a strong association with SHIP and a weak association with SHP-1 and SHP-2 in the MOLT4 cell line which is a T-cell leukemia cell line expressing CD112R (Zhu et al., 2016). Furthermore, Whelan et. al. observed – which is in line with the results of this study – a high (60%-80%) fraction of CD8⁺ cytotoxic T-cells showing CD112R expression, while co-expression of CD112R and PD-1 was seen markedly more infrequent in T-cells (44% of CD8⁺ T-cells as well as 20% of CD4⁺ T-cells) (Whelan et al., 2019). Given that it has been documented that the localization, proximity between PD-1⁺ and PD-L1⁺ cells, as well as the abundance of preexisting inhibitory immune checkpoint receptor expression on TILs were strong predictors for response to immune checkpoint therapy (Tumeh et al., 2014). The expression level of both immune checkpoints on CD8⁺ cytotoxic T-cells located in T-cell niches might predict response to such dual immune checkpoint blockade.

In conclusion, CD8⁺ cytotoxic T-cells with high CD112R and PD-1 expression levels are orchestrated in T-cell niches of colorectal cancer and predict prolonged overall survival which emphasizes an important role of T-cell niches in the anti-tumor immune reaction. Therefore, this study provides a rationale for dual immune checkpoint blockade with anti-CD112R and anti-PD-1 therapy in T-cell niche rich colorectal cancers.

5. Summary

Emerging evidence suggests that spatial T-cell organization is a key component for the characterization of the tumor immune microenvironment, to predict response to immune checkpoint therapies and to predict patient's outcome in colorectal cancer. However, only little is known about the spatial organization of immune checkpoint expression on T-cells and the spatial relationship of clinically relevant novel immune checkpoint receptors (e.g., PD-1 and CD112R). Just recently, combined immune checkpoint blockade directed against PD-1 and CD112R showed clinical benefit rates of 75% in several advanced tumor entities and also partial response – in commonly non-responsive – microsatellite-stable colorectal cancer.

To assess the expression level and spatial orchestration of CD112R and PD-1 on proliferating (Ki67⁺) as well as non-proliferating (Ki67⁻) CD8⁺ T-cells in a historical cohort of 523 colorectal cancers, a deep learning-based framework for automated T-cell-niche identification using multiplex fluorescence immunohistochemistry was developed and applied in this study.

The data revealed that the spatial analysis of locally enriched CD8⁺ T-cell densities and cell-to-cell contacts is a hallmark of T-cell-niches in the tumor microenvironment of colorectal cancer. CD112R and PD-1 expression on CD8⁺ T-cells located in T-cell-niches was found elevated compared to all other tumor compartments ($p < 0.001$ each). Although the highest mean CD112R expression on CD8⁺ T-cells was observed at the invasive margin, the PD-1 expression on CD8⁺ T-cells was elevated in the center of the tumor ($p < 0.001$ each). Across all tissue compartments, proliferating CD8⁺ T-cells showed higher relative CD112R and PD-1 expression compared to the non-proliferating CD8⁺ T-cell subset ($p < 0.001$ each). Integration of all available spatial and immune checkpoint expression parameters (AUC: 0.65) revealed a superior predictive performance for overall survival compared to the commonly used CD8⁺ TILs density (AUC 0.57, $p < 0.001$). In conclusion, cytotoxic T-cells with elevated CD112R and PD-1 expression levels are orchestrated in T-cells niches in colorectal cancer and predict favorable patient's outcome. Proliferation of CD8⁺ T-cells is associated with elevated CD112R and PD-1 expression levels across all tissue compartments. Therefore, the data from this study provide a rationale for dual immune checkpoint blockade with anti-CD112R and anti-PD-1 therapy in T-cell niche rich colorectal cancers.

6. Zusammenfassung

Neue Erkenntnisse deuten darauf hin, dass die räumlichen T-Zell-Verteilungsmuster eine Schlüsselkomponente für die Charakterisierung der Tumor-Immun-Mikroumgebung und das Ansprechen auf Immun-Checkpoint-Therapien, im Darmkrebs, darstellt. Über die räumliche Organisation der Immuncheckpoint-Expression auf T-Zellen und die räumliche Beziehung klinisch relevanter neuer Immuncheckpoint-Rezeptoren (z. B. PD-1 und CD112R) ist jedoch nur wenig bekannt. Erst kürzlich zeigte eine kombinierte Immun-Checkpoint-Blockade gegen PD-1 und CD112R klinische Nutzenraten von 75 % bei mehreren fortgeschrittenen Tumorentitäten, sowie ein partielles Ansprechen bei – meist nicht ansprechendem – Mikrosatelliten-stabilem kolorektalen Karzinom.

Zur Bewertung des Expressionsniveaus und der räumlichen Verteilung von CD112R und PD-1 auf proliferierenden (Ki67⁺) sowie nicht proliferierenden (Ki67⁻) CD8⁺ T-Zellen in einer historischen Kohorte von 523 kolorektalen Karzinomen, wurde ein auf Deep Learning basierender Algorithmus für die automatisierte T-Zell-Nest-Identifizierung mittels Multiplex-Fluoreszenz-Immunhistochemie entwickelt und in dieser Studie angewendet.

Die Daten zeigten, dass lokal erhöhte CD8⁺ T-Zelldichte, welche mit einer lokal erhöhten Anzahl von Zell-zu-Zell-Kontakten einhergeht, ein Charakteristikum der T-Zell-Nester in der Tumormikroumgebung von Darmkrebs darstellt. Die Expression von CD112R und PD-1 auf CD8⁺ T-Zellen, die sich in T-Zell-Nestern befinden, war im Vergleich zu allen anderen Tumorkompartimenten signifikant erhöht (jeweils $p < 0,001$). Obwohl die höchste mittlere CD112R-Expression auf CD8⁺ T-Zellen an der Invasionsfront des Tumors beobachtet wurde, war die PD-1-Expression auf CD8⁺ T-Zellen im Zentrum des Tumors erhöht (jeweils $p < 0,001$). Über alle Gewebekompartimente hinweg zeigten proliferierende CD8⁺ T-Zellen eine höhere relative CD112R- und PD-1-Expression im Vergleich zur nicht proliferierenden CD8⁺ T-Zell-Untergruppen (jeweils $p < 0,001$). Die Integration aller verfügbaren räumlichen und Immun-Checkpoint-Expressionsparameter (AUC: 0,65) zeigte eine überlegene Vorhersageleistung für das Gesamtüberleben im Vergleich zur üblicherweise verwendeten CD8⁺ T-Zell-Dichte (AUC 0,57, $p < 0,001$). Zusammenfassend lässt sich sagen, dass zytotoxische T-Zellen mit erhöhten CD112R- und PD-1-Expressionsniveaus sich räumlich in T-Zell-Nestern anordnen und mit einer günstigen Prognose von Darmkrebspatienten assoziiert sind. Die Proliferation von CD8⁺ T-Zellen geht mit einer erhöhten CD112R- und PD-1-Expressionsniveaus in allen Gewebekompartimenten einher. Daher liefern die Daten aus dieser Studie Hinweise für die Wirksamkeit einer dualen Immun-Checkpoint-Blockade mit Anti-CD112R- und Anti-PD-1-Therapie bei T-Zell-Nestern reichen kolorektalen Karzinomen.

7. Abbreviations

APC	<i>Antigen-presenting cells</i>
ATM/ATR	<i>Ataxia-telangiectasia mutated or/and Rad3-related</i>
bfIHC	<i>brightfield-immunohistochemistry</i>
CD	<i>Cluster of Differentiation</i>
CODEX	<i>Co-detection by indexing</i>
CTLA-4	<i>Cytotoxic T-Lymphocyte Antigen 4</i>
CXCL	<i>Chemokine (C-X-C motif) ligand</i>
DAPI	<i>Diamidin-2-phenylindol</i>
DMEM	<i>Dulbecco's Modified Eagle's Medium</i>
DNAM-1	<i>DNAX Accessory Molecule-1, auch CD226</i>
i.e.,	<i>id est</i>
e.g.,	<i>exempli gratia</i>
ELISA	<i>Enzyme-linked Immunosorbent Assay</i>
FBS	<i>Fetal bovine serum</i>
FDA	<i>Food and Drug Administration</i>
GM-CSF	<i>Granulocyte-macrophage colony-stimulating factor</i>
HE	<i>Hematoxylin and eosin</i>
<i>Hela</i>	<i>Human cervix epithelial carcinoma cells</i>
<i>IFN</i>	<i>Interferon</i>
irAEs	<i>immune-related adverse events</i>
ITIM	<i>Immunoreceptor tyrosin-based inhibitory motifs</i>
mflHC	<i>multiplex-fluorescence-immunohistochemistry</i>
MSI/dMMR	<i>Microsatellite instability and/or mismatch-repair deficiency</i>
MSS/pMMR	<i>Microsatellite stability and/or mismatch-repair proficient</i>
mRNA	<i>messenger ribonuclear acid</i>
NFAT	<i>Nuclear factor of activated T-cells</i>
NK-cells	<i>Natural killer cells</i>
PBS	<i>Phosphate buffered saline</i>
PD-1	<i>Programmed cell death protein 1</i>
PD-L1	<i>Programmed cell death 1 ligand 1</i>
PVR	<i>Poliovirus receptor, also CD155</i>
PVRIG	<i>Poliovirus receptor-related immunoglobulin domain-containing, also CD112R</i>
RT-PCR	<i>Reverse transcriptase-polymerase chain reaction</i>
ROC	<i>Time-dependent receiver operating characteristic</i>
TACTILE	<i>T-cell-activated increased late expression, also CD96</i>

TCF	<i>T-cell factor</i>
TCR	<i>T-cell receptor</i>
TIGIT	<i>T-cell immunoreceptor with Ig and ITIM domains</i>
TILs	<i>Tumor-infiltrated lymphocytes</i>
TLS	<i>Tertiary lymphoid structures</i>
TMA	<i>Tissue MicroArray</i>
TME	<i>Tumor Microenvironment</i>
TPEX	<i>Precursors of exhausted T-cells</i>
TSA	<i>Tyramine signal amplification</i>
t-SNE	<i>T-distributed stochastic neighbor embedding</i>

8. List of Figures

Figure 1: Interaction network between the immune checkpoint receptors (blue) and their ligands (green). The size of the arrows indicates the affinity of the interaction.....	11
Figure 2: The representative multiplex fluorescence immunohistochemistry image of a large section is displayed. The virtual TMA grid (50 cores) is applied to mimic the TMA segmentation, one core represents one punch (top). The CD8 ⁺ density of each punch and overall density of the large section is calculated (bottom).....	17
Figure 3: The representative reference TMA image (A) and reference TMA layout (B) are displayed.	18
Figure 4: Automated T-cell niche detection by the combination of local density measurements and a deep learning-based cell detection. The highest accuracy of T-cell niche detection was achieved by calculating the local density of index cells at a 20µm radius. For this purpose, 20 annotations of niche and non-niche were made by a pathologist.	22
Figure 5: Representative CD8 ⁺ cytotoxic T-cell with high CD112R expression (top), high PD-1 expression (middle), and typical low expression of both immune checkpoints are displayed. (184x magnification).....	24
Figure 6: The raw mIHC image and density heatmaps (CD8 ⁺ T-cell density (red), CD112R relative intensity on CD8 ⁺ T-cells (blue), and PD-1 relative intensity on CD8 ⁺ T-cells (blue)) are shown.....	25
Figure 7: The raw multiplex fluorescence IHC image (left) and the heatmap visualization of automated T-cell niche detection (right) are shown.	26
Figure 8: The expression level of CD112R, PD-1, and Ki67 on the CD8 ⁺ T-cells located in T-cell niches and other tissue compartments (non-niche) are shown according to the t-distributed stochastic neighbor embedding (t-SNE) algorithm. Each point represents a single CD8 ⁺ T-cell sample, and the axes (t-SNE1 and t-SNE2) have arbitrary units. The more similar the samples are, the closer together they appear on the t-SNE plot.	27
Figure 9: Density heatmaps showing the automated T-cell niche detection (pink), CD8 ⁺ T-cell density (red), and CD112R and PD-1 relative intensity (blue) for 3 cases with an inflamed immune phenotype.....	28
Figure 10: Density heatmaps showing the automated T-cell niche detection (pink), CD8 ⁺ T-cell density (red), and CD112R and PD-1 relative intensity (blue) for 3 cases with for 3 cases with a non-inflamed phenotype (bottom).....	28
Figure 11: An unsupervised cluster analysis of the CD8 ⁺ T-cell density (red), cell-to-cell contacts (green), CD112R and PD-1 relative intensity (RE, blue) and proliferation rate of CD8 ⁺ T-cells identified cases with an inflamed (top) as well as with a non-inflamed immune phenotype is depicted.	29
Figure 12: The expression level of CD112R and PD-1 on the proliferating CD8 ⁺ T-cells and non-proliferating CD8 ⁺ T-cells is shown according to the t-SNE algorithm. Each point represents a single CD8 ⁺ T-cell sample, and the axes (t-SNE1 and t-SNE2) have arbitrary units. The more similar the samples are, the closer together they appear on the t-SNE plot.	30

Figure 13: Representative multiplex fluorescence immunohistochemistry images of proliferating CD8 ⁺ T-cells and non-proliferating CD8 ⁺ T-cells in colorectal cancer. The expression of CD8 (orange), Ki67 (red), CD112R (green), and PD-1 (blue) are individually displayed. (184x magnification).....	31
Figure 14: The relative intensity of CD112R is shown significantly increased (***) p<0.001) on the proliferating (black) compared to the non-proliferating (grey) CD8 ⁺ T-cell subset.	32
Figure 15: The relative intensity of PD-1 is shown significantly increased (***) p<0.001) on the proliferating (black) compared to the non-proliferating (grey) CD8 ⁺ T-cell subset.	32
Figure 16: An unsupervised cluster analysis of the fraction of CD8 ⁺ T-cells in niche (pink), CD8 ⁺ T-cells density (red), CD8 ⁺ Ki67 ⁺ density (red), CD8 ⁺ Ki67 ⁻ density (red), CD112R relative intensity on CD8 ⁺ T-cells (blue), and PD-1 relative intensity (blue) on CD8 ⁺ T-cells is depicted.....	34
Figure 17: The Kaplan-Meier Estimates analysis based on the unsupervised cluster (two clusters: a and b and four clusters: a1, a2, b1, and b2) is displayed.	34
Figure 18: Time-dependent receiver operating characteristic curve with niche integrated phenotypes (black) and CD8 ⁺ T-cell density phenotypes (grey) is displayed.	35

9. List of Tables

Table 1: Patient characteristics are shown for the large section cohort.....	14
Table 2: Patient characteristics are shown for the TMA cohort.....	16
Table 3: List of used antibodies, antigen retrieval (AR), dilutions, and Opal dyes for multiplex fluorescence immunohistochemistry.	19
Table 4: Association between relative CD112R and PD-1 expression level and the localization of the CD8 ⁺ T-cells.	30
Table 5: Univariate analysis of fraction of CD8 ⁺ T-cells in niche, CD112R relative intensity on CD8 ⁺ T-cells, PD-1 relative intensity on CD8 ⁺ T-cells, CD8 ⁺ T-cell density, and fraction of proliferating CD8 ⁺ T-cells is shown.	33

10. References

- AHMADZADEH, M., JOHNSON, L. A., HEEMSKERK, B., WUNDERLICH, J. R., DUDLEY, M. E., WHITE, D. E. & ROSENBERG, S. A. 2009. Tumor antigen-specific CD8 T cells infiltrating the tumor express high levels of PD-1 and are functionally impaired. *Blood*, 114, 1537-44.
- AMBROSI, L., KHAN, S., CARVAJAL, R. D. & YANG, J. 2019. Novel Targets for the Treatment of Melanoma. *Curr Oncol Rep*, 21, 97.
- ANTONIA, S. J., VILLEGAS, A., DANIEL, D., VICENTE, D., MURAKAMI, S., HUI, R., KURATA, T., CHIAPPORI, A., LEE, K. H., DE WIT, M., CHO, B. C., BOURHABA, M., QUANTIN, X., TOKITO, T., MEKHAIL, T., PLANCHARD, D., KIM, Y. C., KARAPETIS, C. S., HIRET, S., OSTOROS, G., KUBOTA, K., GRAY, J. E., PAZ-ARES, L., DE CASTRO CARPENO, J., FAIVRE-FINN, C., RECK, M., VANSTEENKISTE, J., SPIGEL, D. R., WADSWORTH, C., MELILLO, G., TABOADA, M., DENNIS, P. A., OZGUROGLU, M. & INVESTIGATORS, P. 2018. Overall Survival with Durvalumab after Chemoradiotherapy in Stage III NSCLC. *N Engl J Med*, 379, 2342-2350.
- ARBOUR, K. C., MEZQUITA, L., LONG, N., RIZVI, H., AUCLIN, E., NI, A., MARTINEZ-BERNAL, G., FERRARA, R., LAI, W. V., HENDRIKS, L. E. L., SABARI, J. K., CAMELLA, C., PLODKOWSKI, A. J., HALPENNY, D., CHAFT, J. E., PLANCHARD, D., RIELY, G. J., BESSE, B. & HELLMANN, M. D. 2018. Impact of Baseline Steroids on Efficacy of Programmed Cell Death-1 and Programmed Death-Ligand 1 Blockade in Patients With Non-Small-Cell Lung Cancer. *J Clin Oncol*, 36, 2872-2878.
- ARORA, S., VELICHINSKII, R., LESH, R. W., ALI, U., KUBIAK, M., BANSAL, P., BORGHAEI, H., EDELMAN, M. J. & BOUMBER, Y. 2019. Existing and Emerging Biomarkers for Immune Checkpoint Immunotherapy in Solid Tumors. *Adv Ther*, 36, 2638-2678.
- BAGCHI, S., YUAN, R. & ENGLEMAN, E. G. 2021. Immune Checkpoint Inhibitors for the Treatment of Cancer: Clinical Impact and Mechanisms of Response and Resistance. *Annu Rev Pathol*, 16, 223-249.
- BARETTI, M. & LE, D. T. 2018. DNA mismatch repair in cancer. *Pharmacol Ther*, 189, 45-62.
- BASHASHATI, A. & BRINKMAN, R. R. 2009. A survey of flow cytometry data analysis methods. *Adv Bioinformatics*, 584603.
- BERNTSSON, J., EBERHARD, J., NODIN, B., LEANDERSSON, K., LARSSON, A. H. & JIRSTROM, K. 2018. Expression of programmed cell death protein 1 (PD-1) and its ligand PD-L1 in colorectal cancer: Relationship with sidedness and prognosis. *Oncoimmunology*, 7, e1465165.
- BILLADEAU, D. D. & LEIBSON, P. J. 2002. ITAMs versus ITIMs: striking a balance during cell regulation. *J Clin Invest*, 109, 161-8.
- BLANCHE, P., DARTIGUES, J. F. & JACQMIN-GADDA, H. 2013. Estimating and comparing time-dependent areas under receiver operating characteristic curves for censored event times with competing risks. *Stat Med*, 32, 5381-97.
- BLESSIN, N. C., CHENG, Y., MANDELKOW, T., RAEDLER, J. B., LI, W., BADY, E., SIMON, R., VETTORAZZI, E., LENNARTZ, M., BERNREUTHER, C., FRAUNE, C., JACOBSEN, F., KRECH, T., MARX, A., LEBOK, P., MINNER, S., BURANDT, E., CLAUDITZ, S. T., WILCZAK, W., SAUTER, G., HEINZER, H., HAESE, A., SCHLOMM, T., GRAEFEN, M. & STEURER, S. 2021a. Automated Ki67-LI assessment in prostate cancer using artificial intelligence in multiplex fluorescence immunohistochemistry *European Urology (submitted)*.

- BLESSIN, N. C., JANSEN, H. L., LI, W., MANDELKOW, T., YANG, C., SIMON, R., HOFFMANN, C., BERNREUTHER, C., LEBOK, P., BÜSCHECK, F., SAUTER, G., LUEBKE, A., UHLIG, R., WALDEMAR, W., WEIDEMANN, S., KLUTH, M., CLAUDITZ, T., FRAUNE, C., DUM, D., HINSCH, A., HÖFLMAYER, D., KRECH, T., MARX, A., MINNER, S., BURANDT, E. & STEURER, S. 2021b. Deep profiling revealed an upregulation of CD112R in human cancer *Cancer Immunology Research* (submitted).
- BLESSIN, N. C., LI, W., MANDELKOW, T., JANSEN, H. L., YANG, C., RAEDLER, J. B., SIMON, R., BUSCHECK, F., DUM, D., LUEBKE, A. M., HINSCH, A., MOLLER, K., MENZ, A., BERNREUTHER, C., LEBOK, P., CLAUDITZ, T., SAUTER, G., MARX, A., UHLIG, R., WILCZAK, W., MINNER, S., KRECH, T., FRAUNE, C., HOFLMAYER, D., BURANDT, E. & STEURER, S. 2021c. Prognostic role of proliferating CD8(+) cytotoxic T cells in human cancers. *Cell Oncol (Dordr)*.
- BLESSIN, N. C., SIMON, R., KLUTH, M., FISCHER, K., HUBE-MAGG, C., LI, W., MAKRYPIDI-FRAUNE, G., WELLGE, B., MANDELKOW, T., DEBATIN, N. F., HOFLMAYER, D., LENNARTZ, M., SAUTER, G., IZBICKI, J. R., MINNER, S., BUSCHECK, F., UHLIG, R., DUM, D., KRECH, T., LUEBKE, A. M., WITTMER, C., JACOBSEN, F., BURANDT, E. C., STEURER, S., WILCZAK, W. & HINSCH, A. 2019. Patterns of TIGIT Expression in Lymphatic Tissue, Inflammation, and Cancer. *Dis Markers*, 2019, 5160565.
- BLESSIN, N. C., SPRIESTERSBACH, P., LI, W., MANDELKOW, T., DUM, D., SIMON, R., HUBE-MAGG, C., LUTZ, F., VIEHWEGER, F., LENNARTZ, M., FRAUNE, C., NICKELSEN, V., FEHRLE, W., GOBEL, C., WEIDEMANN, S., CLAUDITZ, T., LEBOK, P., MOLLER, K., STEURER, S., IZBICKI, J. R., SAUTER, G., MINNER, S., JACOBSEN, F., LUEBKE, A. M., BUSCHECK, F., HOFLMAYER, D., WILCZAK, W., BURANDT, E. & HINSCH, A. 2020. Prevalence of CD8(+) cytotoxic lymphocytes in human neoplasms. *Cell Oncol (Dordr)*, 43, 421-430.
- BORGHAEI, H., PAZ-ARES, L., HORN, L., SPIGEL, D. R., STEINS, M., READY, N. E., CHOW, L. Q., VOKES, E. E., FELIP, E., HOLGADO, E., BARLESI, F., KOHLHAUFL, M., ARRIETA, O., BURGIO, M. A., FAYETTE, J., LENA, H., PODDUBSKAYA, E., GERBER, D. E., GETTINGER, S. N., RUDIN, C. M., RIZVI, N., CRINO, L., BLUMENSCHNEIN, G. R., JR., ANTONIA, S. J., DORANGE, C., HARBISON, C. T., GRAF FINCKENSTEIN, F. & BRAHMER, J. R. 2015. Nivolumab versus Docetaxel in Advanced Nonsquamous Non-Small-Cell Lung Cancer. *N Engl J Med*, 373, 1627-39.
- BOWERS, J. R., READLER, J. M., SHARMA, P. & EXCOFFON, K. 2017. Poliovirus Receptor: More than a simple viral receptor. *Virus Res*, 242, 1-6.
- BOYIADZIS, M. M., KIRKWOOD, J. M., MARSHALL, J. L., PRITCHARD, C. C., AZAD, N. S. & GULLEY, J. L. 2018. Significance and implications of FDA approval of pembrolizumab for biomarker-defined disease. *J Immunother Cancer*, 6, 35.
- BUDER-BAKHAYA, K. & HASSEL, J. C. 2018. Biomarkers for Clinical Benefit of Immune Checkpoint Inhibitor Treatment-A Review From the Melanoma Perspective and Beyond. *Front Immunol*, 9, 1474.
- CABRITA, R., LAUSS, M., SANNA, A., DONIA, M., SKAARUP LARSEN, M., MITRA, S., JOHANSSON, I., PHUNG, B., HARBST, K., VALLON-CHRISTERSSON, J., VAN SCHOIACK, A., LOVGREN, K., WARREN, S., JIRSTROM, K., OLSSON, H., PIETRAS, K., INGVAR, C., ISAKSSON, K., SCHADENDORF, D., SCHMIDT, H., BASTHOLT, L., CARNEIRO, A., WARGO, J. A., SVANE, I.

- M. & JONSSON, G. 2020. Tertiary lymphoid structures improve immunotherapy and survival in melanoma. *Nature*, 577, 561-565.
- CAO, X. H., STOJKOVIC, I. & OBRADOVIC, Z. 2016. A robust data scaling algorithm to improve classification accuracies in biomedical data. *BMC Bioinformatics*, 17, 359.
- CAREY, C. D., GUSENLEITNER, D., LIPSCHITZ, M., ROEMER, M. G. M., STACK, E. C., GJINI, E., HU, X., REDD, R., FREEMAN, G. J., NEUBERG, D., HODI, F. S., LIU, X. S., SHIPP, M. A. & RODIG, S. J. 2017. Topological analysis reveals a PD-L1-associated microenvironmental niche for Reed-Sternberg cells in Hodgkin lymphoma. *Blood*, 130, 2420-2430.
- CHAUVIN, J. M. & ZAROOUR, H. M. 2020. TIGIT in cancer immunotherapy. *J Immunother Cancer*, 8.
- CHEN, D. S. & MELLMAN, I. 2017. Elements of cancer immunity and the cancer-immune set point. *Nature*, 541, 321-330.
- COHEN, R., ROUSSEAU, B., VIDAL, J., COLLE, R., DIAZ, L. A., JR. & ANDRE, T. 2020. Immune Checkpoint Inhibition in Colorectal Cancer: Microsatellite Instability and Beyond. *Target Oncol*, 15, 11-24.
- COUZIN-FRANKEL, J. 2013. Cancer immunotherapy. American Association for the Advancement of Science.
- CUYLEN, S., BLAUKOPF, C., POLITI, A. Z., MULLER-REICHERT, T., NEUMANN, B., POSER, I., ELLENBERG, J., HYMAN, A. A. & GERLICH, D. W. 2016. Ki-67 acts as a biological surfactant to disperse mitotic chromosomes. *Nature*, 535, 308-12.
- DI CARO, G., BERGOMAS, F., GRIZZI, F., DONI, A., BIANCHI, P., MALESCI, A., LAGHI, L., ALLAVENA, P., MANTOVANI, A. & MARCHESI, F. 2014. Occurrence of tertiary lymphoid tissue is associated with T-cell infiltration and predicts better prognosis in early-stage colorectal cancers. *Clin Cancer Res*, 20, 2147-58.
- DIGGS, L. P. & HSUEH, E. C. 2017. Utility of PD-L1 immunohistochemistry assays for predicting PD-1/PD-L1 inhibitor response. *Biomark Res*, 5, 12.
- DUFFY, M. J. & CROWN, J. 2019. Biomarkers for Predicting Response to Immunotherapy with Immune Checkpoint Inhibitors in Cancer Patients. *Clin Chem*, 65, 1228-1238.
- DUNN, G. P., BRUCE, A. T., IKEDA, H., OLD, L. J. & SCHREIBER, R. D. 2002. Cancer immunoediting: from immunosurveillance to tumor escape. *Nat Immunol*, 3, 991-8.
- FOUNDATION, P. S. 2021. Python Language Reference, . Available at <http://www.python.org>.
- GALON, J., COSTES, A., SANCHEZ-CABO, F., KIRILOVSKY, A., MLECNIK, B., LAGORCE-PAGES, C., TOSOLINI, M., CAMUS, M., BERGER, A., WIND, P., ZINZINDOHOUE, F., BRUNEVAL, P., CUGNENC, P. H., TRAJANOSKI, Z., FRIDMAN, W. H. & PAGES, F. 2006. Type, density, and location of immune cells within human colorectal tumors predict clinical outcome. *Science*, 313, 1960-4.
- GARON, E. B., RIZVI, N. A., HUI, R., LEIGHL, N., BALMANOUKIAN, A. S., EDER, J. P., PATNAIK, A., AGGARWAL, C., GUBENS, M., HORN, L., CARCERENY, E., AHN, M. J., FELIP, E., LEE, J. S., HELLMANN, M. D., HAMID, O., GOLDMAN, J. W., SORIA, J. C., DOLLED-FILHART, M., RUTLEDGE, R. Z., ZHANG, J., LUNCEFORD, J. K., RANGWALA, R., LUBINIECKI, G. M., ROACH, C., EMANCIPATOR, K., GANDHI, L. & INVESTIGATORS, K.-. 2015.

- Pembrolizumab for the treatment of non-small-cell lung cancer. *N Engl J Med*, 372, 2018-28.
- GIBNEY, G. T., WEINER, L. M. & ATKINS, M. B. 2016. Predictive biomarkers for checkpoint inhibitor-based immunotherapy. *Lancet Oncol*, 17, e542-e551.
- GOLTSEV, Y., SAMUSIK, N., KENNEDY-DARLING, J., BHATE, S., HALE, M., VAZQUEZ, G., BLACK, S. & NOLAN, G. P. 2018. Deep Profiling of Mouse Splenic Architecture with CODEX Multiplexed Imaging. *Cell*, 174, 968-981 e15.
- GORVEL, L. & OLIVE, D. 2020. Targeting the "PVR-TIGIT axis" with immune checkpoint therapies. *F1000Res*, 9.
- HARGADON, K. M., JOHNSON, C. E. & WILLIAMS, C. J. 2018. Immune checkpoint blockade therapy for cancer: An overview of FDA-approved immune checkpoint inhibitors. *Int Immunopharmacol*, 62, 29-39.
- HARJUNPAA, H. & GUILLEREY, C. 2020. TIGIT as an emerging immune checkpoint. *Clin Exp Immunol*, 200, 108-119.
- HAVEL, J. J., CHOWELL, D. & CHAN, T. A. 2019. The evolving landscape of biomarkers for checkpoint inhibitor immunotherapy. *Nat Rev Cancer*, 19, 133-150.
- HE, Y., BOWMAN, V. D., MUELLER, S., BATOR, C. M., BELLA, J., PENG, X., BAKER, T. S., WIMMER, E., KUHN, R. J. & ROSSMANN, M. G. 2000. Interaction of the poliovirus receptor with poliovirus. *Proceedings of the National Academy of Sciences*, 97, 79-84.
- HELLMANN, M. D., CIULEANU, T. E., PLUZANSKI, A., LEE, J. S., OTTERSON, G. A., AUDIGIER-VALETTE, C., MINENZA, E., LINARDOU, H., BURGERS, S., SALMAN, P., BORGHAEI, H., RAMALINGAM, S. S., BRAHMER, J., RECK, M., O'BYRNE, K. J., GEESE, W. J., GREEN, G., CHANG, H., SZUSTAKOWSKI, J., BHAGAVATHEESWARAN, P., HEALEY, D., FU, Y., NATHAN, F. & PAZ-ARES, L. 2018. Nivolumab plus Ipilimumab in Lung Cancer with a High Tumor Mutational Burden. *N Engl J Med*, 378, 2093-2104.
- HODI, F. S., CHIARION-SILENI, V., GONZALEZ, R., GROB, J. J., RUTKOWSKI, P., COWEY, C. L., LAO, C. D., SCHADENDORF, D., WAGSTAFF, J., DUMMER, R., FERRUCCI, P. F., SMYLLIE, M., HILL, A., HOGG, D., MARQUEZ-RODAS, I., JIANG, J., RIZZO, J., LARKIN, J. & WOLCHOK, J. D. 2018. Nivolumab plus ipilimumab or nivolumab alone versus ipilimumab alone in advanced melanoma (CheckMate 067): 4-year outcomes of a multicentre, randomised, phase 3 trial. *Lancet Oncol*, 19, 1480-1492.
- HUNG, A. L., MAXWELL, R., THEODROS, D., BELCAID, Z., MATHIOS, D., LUKSIK, A. S., KIM, E., WU, A., XIA, Y., GARZON-MUVDI, T., JACKSON, C., YE, X., TYLER, B., SELBY, M., KORMAN, A., BARNHART, B., PARK, S. M., YOUN, J. I., CHOWDHURY, T., PARK, C. K., BREM, H., PARDOLL, D. M. & LIM, M. 2018. TIGIT and PD-1 dual checkpoint blockade enhances antitumor immunity and survival in GBM. *Oncoimmunology*, 7, e1466769.
- JANSEN, C. S., PROKHNEVSKA, N., MASTER, V. A., SANDA, M. G., CARLISLE, J. W., BILEN, M. A., CARDENAS, M., WILKINSON, S., LAKE, R., SOWALSKY, A. G., VALANPARAMBIL, R. M., HUDSON, W. H., MCGUIRE, D., MELNICK, K., KHAN, A. I., KIM, K., CHANG, Y. M., KIM, A., FILSON, C. P., ALEMOZAFFAR, M., OSUNKOYA, A. O., MULLANE, P., ELLIS, C., AKONDY, R., IM, S. J., KAMPHORST, A. O., REYES, A., LIU, Y. & KISSICK, H. 2019. An intra-tumoral niche maintains and differentiates stem-like CD8 T cells. *Nature*, 576, 465-470.

- JOHNSON, D. E., BURTNESSE, B., LEEMANS, C. R., LUI, V. W. Y., BAUMAN, J. E. & GRANDIS, J. R. 2020. Head and neck squamous cell carcinoma. *Nat Rev Dis Primers*, 6, 92.
- KAMPHORST, A. O., PILLAI, R. N., YANG, S., NASTI, T. H., AKONDY, R. S., WIELAND, A., SICA, G. L., YU, K., KOENIG, L., PATEL, N. T., BEHERA, M., WU, H., MCCAUSLAND, M., CHEN, Z., ZHANG, C., KHURI, F. R., OWONIKOKO, T. K., AHMED, R. & RAMALINGAM, S. S. 2017. Proliferation of PD-1+ CD8 T cells in peripheral blood after PD-1-targeted therapy in lung cancer patients. *Proc Natl Acad Sci U S A*, 114, 4993-4998.
- KEIR, M. E., BUTTE, M. J., FREEMAN, G. J. & SHARPE, A. H. 2008. PD-1 and its ligands in tolerance and immunity. *Annu Rev Immunol*, 26, 677-704.
- KENNEDY, L. B. & SALAMA, A. K. S. 2020. A review of cancer immunotherapy toxicity. *CA Cancer J Clin*, 70, 86-104.
- KOBAK, D. & BERENS, P. 2019. The art of using t-SNE for single-cell transcriptomics. *Nat Commun*, 10, 5416.
- KONONEN, J., BUBENDORF, L., KALLIONIEMI, A., BARLUND, M., SCHRAML, P., LEIGHTON, S., TORHORST, J., MIHATSCH, M. J., SAUTER, G. & KALLIONIEMI, O. P. 1998. Tissue microarrays for high-throughput molecular profiling of tumor specimens. *Nat Med*, 4, 844-7.
- LARKIN, J., CHIARION-SILENI, V., GONZALEZ, R., GROB, J. J., COWEY, C. L., LAO, C. D., SCHADENDORF, D., DUMMER, R., SMYLLIE, M., RUTKOWSKI, P., FERRUCCI, P. F., HILL, A., WAGSTAFF, J., CARLINO, M. S., HAANEN, J. B., MAIO, M., MARQUEZ-RODAS, I., MCARTHUR, G. A., ASCIERTO, P. A., LONG, G. V., CALLAHAN, M. K., POSTOW, M. A., GROSSMANN, K., SZNOL, M., DRENO, B., BASTHOLT, L., YANG, A., ROLLIN, L. M., HORAK, C., HODI, F. S. & WOLCHOK, J. D. 2015. Combined Nivolumab and Ipilimumab or Monotherapy in Untreated Melanoma. *N Engl J Med*, 373, 23-34.
- LAUSS, M., DONIA, M., HARBST, K., ANDERSEN, R., MITRA, S., ROSENGREN, F., SALIM, M., VALLON-CHRISTERSSON, J., TORNGREN, T., KVIST, A., RINGNER, M., SVANE, I. M. & JONSSON, G. 2017. Mutational and putative neoantigen load predict clinical benefit of adoptive T cell therapy in melanoma. *Nat Commun*, 8, 1738.
- LE, D. T., URAM, J. N., WANG, H., BARTLETT, B. R., KEMBERLING, H., EYRING, A. D., SKORA, A. D., LUBER, B. S., AZAD, N. S., LAHERU, D., BIEDRZYCKI, B., DONEHOWER, R. C., ZAHEER, A., FISHER, G. A., CROCENZI, T. S., LEE, J. J., DUFFY, S. M., GOLDBERG, R. M., DE LA CHAPELLE, A., KOSHIJI, M., BHAIJEE, F., HUEBNER, T., HRUBAN, R. H., WOOD, L. D., CUKA, N., PARDOLL, D. M., PAPADOPOULOS, N., KINZLER, K. W., ZHOU, S., CORNISH, T. C., TAUBE, J. M., ANDERS, R. A., ESHLEMAN, J. R., VOGELSTEIN, B. & DIAZ, L. A., JR. 2015. PD-1 Blockade in Tumors with Mismatch-Repair Deficiency. *N Engl J Med*, 372, 2509-20.
- LENTZ, R. W., COLTON, M. D., MITRA, S. S. & MESSERSMITH, W. A. 2021. Innate immune checkpoint inhibitors: the next breakthrough in medical oncology? *Molecular Cancer Therapeutics*, 20, 961-974.
- LIN, A., ZHANG, J. & LUO, P. 2020. Crosstalk Between the MSI Status and Tumor Microenvironment in Colorectal Cancer. *Front Immunol*, 11, 2039.
- LIU, X., GIBBONS, R. M., HARRINGTON, S. M., KRICO, C. J., MARKOVIC, S. N., KWON, E. D. & DONG, H. 2013. Endogenous tumor-reactive CD8(+) T cells are differentiated effector cells expressing high levels of CD11a and PD-1 but are unable to control tumor growth. *Oncoimmunology*, 2, e23972.

- LUTZ, E., YEO, C. J., LILLEMOR, K. D., BIEDRZYCKI, B., KOBRIN, B., HERMAN, J., SUGAR, E., PIANTADOSI, S., CAMERON, J. L., SOLT, S., ONNERS, B., TARTAKOVSKY, I., CHOI, M., SHARMA, R., ILLEI, P. B., HRUBAN, R. H., ABRAMS, R. A., LE, D., JAFFEE, E. & LAHERU, D. 2011. A lethally irradiated allogeneic granulocyte-macrophage colony stimulating factor-secreting tumor vaccine for pancreatic adenocarcinoma. A Phase II trial of safety, efficacy, and immune activation. *Ann Surg*, 253, 328-35.
- MA, W., GILLIGAN, B. M., YUAN, J. & LI, T. 2016. Current status and perspectives in translational biomarker research for PD-1/PD-L1 immune checkpoint blockade therapy. *J Hematol Oncol*, 9, 47.
- MANDELKOW, T., BLESSIN, N. C., LUEERSS, E., POTT, L., SIMON, R., LI, W., WELLGE, B., DEBATIN, N. F., HOFLMAYER, D., IZBICKI, J. R., BUSCHECK, F., LUEBKE, A. M., WITTMER, C., JACOBSEN, F., LUTZ, F., BURANDT, E., STEURER, S., SAUTER, G., TSOURLAKIS, M. C., WILCZAK, W., HINSCH, A. & MINNER, S. 2019. Immune Exclusion Is Frequent in Small-Cell Carcinoma of the Bladder. *Dis Markers*, 2019, 2532518.
- MCLANE, L. M., ABDEL-HAKEEM, M. S. & WHERRY, E. J. 2019. CD8 T Cell Exhaustion During Chronic Viral Infection and Cancer. *Annu Rev Immunol*, 37, 457-495.
- MCMULLEN, T. P., LAI, R., DABBAGH, L., WALLACE, T. M. & DE GARA, C. J. 2010. Survival in rectal cancer is predicted by T cell infiltration of tumour-associated lymphoid nodules. *Clin Exp Immunol*, 161, 81-8.
- MEHRA, R., SEIWERT, T. Y., GUPTA, S., WEISS, J., GLUCK, I., EDER, J. P., BURTNES, B., TAHARA, M., KEAM, B., KANG, H., MURO, K., GEVA, R., CHUNG, H. C., LIN, C. C., AURORA-GARG, D., RAY, A., PATHIRAJA, K., CHENG, J., CHOW, L. Q. M. & HADDAD, R. 2018. Efficacy and safety of pembrolizumab in recurrent/metastatic head and neck squamous cell carcinoma: pooled analyses after long-term follow-up in KEYNOTE-012. *Br J Cancer*, 119, 153-159.
- METI, N., ESFAHANI, K. & JOHNSON, N. A. 2018. The Role of Immune Checkpoint Inhibitors in Classical Hodgkin Lymphoma. *Cancers (Basel)*, 10.
- MLECNIK, B., BINDEA, G., ANGELL, H. K., MABY, P., ANGELOVA, M., TOUGERON, D., CHURCH, S. E., LAFONTAINE, L., FISCHER, M., FREDRIKSEN, T., SASSO, M., BILOCQ, A. M., KIRILOVSKY, A., OBENAU, A. C., HAMIEH, M., BERGER, A., BRUNEVAL, P., TUECH, J. J., SABOURIN, J. C., LE PESSOT, F., MAUILLON, J., RAFII, A., LAURENT-PUIG, P., SPEICHER, M. R., TRAJANOSKI, Z., MICHEL, P., SESBOUE, R., FREBOURG, T., PAGES, F., VALGE-ARCHER, V., LATOUCHE, J. B. & GALON, J. 2016. Integrative Analyses of Colorectal Cancer Show Immunoscore Is a Stronger Predictor of Patient Survival Than Microsatellite Instability. *Immunity*, 44, 698-711.
- MURTER, B., PAN, X., OPHIR, E., ALTEBER, Z., AZULAY, M., SEN, R., LEVY, O., DASSA, L., VAKNIN, I., FRIDMAN-KFIR, T., SALOMON, R., RAVET, A., TAM, A., LEVIN, D., VAKNIN, Y., TATIROVSKY, E., MACHLENKIN, A., PARDOLL, D. & GANGULY, S. 2019. Mouse PVRIG Has CD8(+) T Cell-Specific Coinhibitory Functions and Dampens Antitumor Immunity. *Cancer Immunol Res*, 7, 244-256.
- OVERMAN, M. J., LONARDI, S., WONG, K. Y. M., LENZ, H. J., GELSOMINO, F., AGLIETTA, M., MORSE, M. A., VAN CUTSEM, E., MCDERMOTT, R., HILL, A., SAWYER, M. B., HENDLISZ, A., NEYNS, B., SVRCEK, M., MOSS, R. A., LEDEINE, J. M., CAO, Z. A., KAMBLE, S., KOPETZ, S. & ANDRE, T. 2018.

- Durable Clinical Benefit With Nivolumab Plus Ipilimumab in DNA Mismatch Repair-Deficient/Microsatellite Instability-High Metastatic Colorectal Cancer. *J Clin Oncol*, 36, 773-779.
- OVERMAN, M. J., MCDERMOTT, R., LEACH, J. L., LONARDI, S., LENZ, H. J., MORSE, M. A., DESAI, J., HILL, A., AXELSON, M., MOSS, R. A., GOLDBERG, M. V., CAO, Z. A., LEDEINE, J. M., MAGLINTE, G. A., KOPETZ, S. & ANDRE, T. 2017. Nivolumab in patients with metastatic DNA mismatch repair-deficient or microsatellite instability-high colorectal cancer (CheckMate 142): an open-label, multicentre, phase 2 study. *Lancet Oncol*, 18, 1182-1191.
- PALUCKA, K. & BANCHEREAU, J. 2013. Dendritic-cell-based therapeutic cancer vaccines. *Immunity*, 39, 38-48.
- PATEL, S. P. & KURZROCK, R. 2015. PD-L1 Expression as a Predictive Biomarker in Cancer Immunotherapy. *Mol Cancer Ther*, 14, 847-56.
- PITZALIS, C., JONES, G. W., BOMBARDIERI, M. & JONES, S. A. 2014. Ectopic lymphoid-like structures in infection, cancer and autoimmunity. *Nat Rev Immunol*, 14, 447-62.
- POSTOW, M. A., SIDLOW, R. & HELLMANN, M. D. 2018. Immune-Related Adverse Events Associated with Immune Checkpoint Blockade. *N Engl J Med*, 378, 158-168.
- QIAO, G. J., CHEN, L., WU, J. C. & LI, Z. R. 2019. Identification of an eight-gene signature for survival prediction for patients with hepatocellular carcinoma based on integrated bioinformatics analysis. *PeerJ*, 7, e6548.
- R-CORE-TEAM 2021. R: A language and environment for statistical computing. *R Foundation for Statistical Computing, Vienna, Austria*. URL <https://www.R-project.org/>.
- RIAZ, N., HAVEL, J. J., MAKAROV, V., DESRICHARD, A., URBA, W. J., SIMS, J. S., HODI, F. S., MARTIN-ALGARRA, S., MANDAL, R., SHARFMAN, W. H., BHATIA, S., HWU, W. J., GAJEWSKI, T. F., SLINGLUFF, C. L., JR., CHOWELL, D., KENDALL, S. M., CHANG, H., SHAH, R., KUO, F., MORRIS, L. G. T., SIDHOM, J. W., SCHNECK, J. P., HORAK, C. E., WEINHOLD, N. & CHAN, T. A. 2017. Tumor and Microenvironment Evolution during Immunotherapy with Nivolumab. *Cell*, 171, 934-949 e16.
- RIAZ, N., MORRIS, L., HAVEL, J. J., MAKAROV, V., DESRICHARD, A. & CHAN, T. A. 2016. The role of neoantigens in response to immune checkpoint blockade. *Int Immunol*, 28, 411-9.
- RIBAS, A. & WOLCHOK, J. D. 2018. Cancer immunotherapy using checkpoint blockade. *Science*, 359, 1350-1355.
- ROBERT, C. 2020. A decade of immune-checkpoint inhibitors in cancer therapy. *Nat Commun*, 11, 3801.
- RODRIGUEZ-ABREU, D., JOHNSON, M. L., HUSSEIN, M. A., COBO, M., PATEL, A. J., SECEN, N. M., LEE, K. H., MASSUTI, B., HIRET, S., YANG, J. C.-H., BARLESI, F., LEE, D. H., PAZ-ARES, L. G., HSIEH, R. W., MILLER, K., PATIL, N., TWOMEY, P., KAPP, A. V., MENG, R. & CHO, B. C. 2020. Primary analysis of a randomized, double-blind, phase II study of the anti-TIGIT antibody tiragolumab (tira) plus atezolizumab (atezo) versus placebo plus atezo as first-line (1L) treatment in patients with PD-L1-selected NSCLC (CITYSCAPE). *Journal of Clinical Oncology*, 38, 9503-9503.
- ROSENBERG, S. A., YANG, J. C. & RESTIFO, N. P. 2004. Cancer immunotherapy: moving beyond current vaccines. *Nat Med*, 10, 909-15.

- SAMSTEIN, R. M., LEE, C. H., SHOUSHARI, A. N., HELLMANN, M. D., SHEN, R., JANJIGIAN, Y. Y., BARRON, D. A., ZEHIR, A., JORDAN, E. J., OMURO, A., KALEY, T. J., KENDALL, S. M., MOTZER, R. J., HAKIMI, A. A., VOSS, M. H., RUSSO, P., ROSENBERG, J., IYER, G., BOCHNER, B. H., BAJORIN, D. F., AL-AHMADIE, H. A., CHAFT, J. E., RUDIN, C. M., RIELY, G. J., BAXI, S., HO, A. L., WONG, R. J., PFISTER, D. G., WOLCHOK, J. D., BARKER, C. A., GUTIN, P. H., BRENNAN, C. W., TABAR, V., MELLINGHOFF, I. K., DEANGELIS, L. M., ARIYAN, C. E., LEE, N., TAP, W. D., GOUNDER, M. M., D'ANGELO, S. P., SALTZ, L., STADLER, Z. K., SCHER, H. I., BASELGA, J., RAZAVI, P., KLEBANOFF, C. A., YAEGER, R., SEGAL, N. H., KU, G. Y., DEMATTEO, R. P., LADANYI, M., RIZVI, N. A., BERGER, M. F., RIAZ, N., SOLIT, D. B., CHAN, T. A. & MORRIS, L. G. T. 2019. Tumor mutational load predicts survival after immunotherapy across multiple cancer types. *Nat Genet*, 51, 202-206.
- SAMUSIK, N., GOOD, Z., SPITZER, M. H., DAVIS, K. L. & NOLAN, G. P. 2016. Automated mapping of phenotype space with single-cell data. *Nat Methods*, 13, 493-6.
- SANCHEZ-CORREA, B., VALHONDO, I., HASSOUNEH, F., LOPEZ-SEJAS, N., PERA, A., BERGUA, J. M., ARCOS, M. J., BANAS, H., CASAS-AVILES, I., DURAN, E., ALONSO, C., SOLANA, R. & TARAZONA, R. 2019. DNAM-1 and the TIGIT/PVRIG/TACTILE Axis: Novel Immune Checkpoints for Natural Killer Cell-Based Cancer Immunotherapy. *Cancers (Basel)*, 11.
- SAUTER, G., SIMON, R. & HILLAN, K. 2003. Tissue microarrays in drug discovery. *Nat Rev Drug Discov*, 2, 962-72.
- SAUTES-FRIDMAN, C., LAWAND, M., GIRALDO, N. A., KAPLON, H., GERMAIN, C., FRIDMAN, W. H. & DIEU-NOSJEAN, M. C. 2016. Tertiary Lymphoid Structures in Cancers: Prognostic Value, Regulation, and Manipulation for Therapeutic Intervention. *Front Immunol*, 7, 407.
- SCHREIBER, R. D., OLD, L. J. & SMYTH, M. J. 2011. Cancer immunoediting: integrating immunity's roles in cancer suppression and promotion. *Science*, 331, 1565-70.
- SERMER, D. & BRENTJENS, R. 2019. CAR T-cell therapy: Full speed ahead. *Hematol Oncol*, 37 Suppl 1, 95-100.
- SHI, J., HOU, S., FANG, Q., LIU, X., LIU, X. & QI, H. 2018. PD-1 Controls Follicular T Helper Cell Positioning and Function. *Immunity*, 49, 264-274 e4.
- SIDDIQUI, I., SCHAEUBLE, K., CHENNUPATI, V., FUERTES MARRACO, S. A., CALDERON-COPETE, S., PAIS FERREIRA, D., CARMONA, S. J., SCARPELLINO, L., GFELLER, D., PRADERVAND, S., LUTHER, S. A., SPEISER, D. E. & HELD, W. 2019. Intratumoral Tcf1(+)PD-1(+)CD8(+) T Cells with Stem-like Properties Promote Tumor Control in Response to Vaccination and Checkpoint Blockade Immunotherapy. *Immunity*, 50, 195-211 e10.
- SOLECKI, D. J., GROMEIER, M., MUELLER, S., BERNHARDT, G. & WIMMER, E. 2002. Expression of the human poliovirus receptor/CD155 gene is activated by sonic hedgehog. *J Biol Chem*, 277, 25697-702.
- SORIANI, A., ZINGONI, A., CERBONI, C., IANNITTO, M. L., RICCIARDI, M. R., DI GIALLEONARDO, V., CIPPITELLI, M., FIONDA, C., PETRUCCI, M. T., GUARINI, A., FOA, R. & SANTONI, A. 2009. ATM-ATR-dependent up-regulation of DNAM-1 and NKG2D ligands on multiple myeloma cells by therapeutic agents results in enhanced NK-cell susceptibility and is associated with a senescent phenotype. *Blood*, 113, 3503-11.

- SPAIN, L., DIEM, S. & LARKIN, J. 2016. Management of toxicities of immune checkpoint inhibitors. *Cancer Treat Rev*, 44, 51-60.
- STACK, E. C., WANG, C., ROMAN, K. A. & HOYT, C. C. 2014. Multiplexed immunohistochemistry, imaging, and quantitation: a review, with an assessment of Tyramide signal amplification, multispectral imaging and multiplex analysis. *Methods*, 70, 46-58.
- SULLIVAN, R., RASCO, D., LIM, E., SHARMA, M., SHEPARD, D., PATNAIK, A., HAMILTON, E., FLEMING, G., PAPADOPOULOS, K., ELNAGGAR, A., ADEWOYE, A. H., CHMIELOWSKI, B., DUMBRAVA, E. & VAENA, D. 2020a. Abstract CT031: COM701 demonstrates preliminary antitumor activity as monotherapy and in combination with nivolumab in patients with advanced solid tumors. *Cancer Research*, 80, CT031-CT031.
- SULLIVAN, R., RASCO, D., LIM, E., SHARMA, M., SHEPARD, D., PATNAIK, A., HAMILTON, E., FLEMING, G., PAPADOPOULOS, K., ELNAGGAR, A., ADEWOYE, A. H., CHMIELOWSKI, B., DUMBRAVA, E. & VAENA, D. 2020b. COM701 Demonstrates Antitumor Activity as Monotherapy and in Combination with Nivolumab in Patients with Advanced Malignancies. *AACR 2020*. Virtual.
- TAKAI, Y., MIYOSHI, J., IKEDA, W. & OGITA, H. 2008. Nectins and nectin-like molecules: roles in contact inhibition of cell movement and proliferation. *Nat Rev Mol Cell Biol*, 9, 603-15.
- TANG, X., SHU, Z., ZHANG, W., CHENG, L., YU, J., ZHANG, M. & ZHENG, S. 2019. Clinical significance of the immune cell landscape in hepatocellular carcinoma patients with different degrees of fibrosis. *Ann Transl Med*, 7, 528.
- THERNEAU, T. M. & GRAMBSCH, P. M. 2000. Modeling Survival Data: Extending the Cox Model. *Springer, New York*, ISBN 0-387-98784-3, <https://CRAN.R-project.org/package=survival>.
- THOMMEN, D. S., KOELZER, V. H., HERZIG, P., ROLLER, A., TREFNY, M., DIMELOE, S., KIIALAINEN, A., HANHART, J., SCHILL, C., HESS, C., SAVIC PRINCE, S., WIESE, M., LARDINOIS, D., HO, P. C., KLEIN, C., KARANIKAS, V., MERTZ, K. D., SCHUMACHER, T. N. & ZIPPELIUS, A. 2018. A transcriptionally and functionally distinct PD-1(+) CD8(+) T cell pool with predictive potential in non-small-cell lung cancer treated with PD-1 blockade. *Nat Med*, 24, 994-1004.
- TIPPMANN, S. 2015. Programming tools: Adventures with R. *Nature*, 517, 109-10.
- TUMEH, P. C., HARVIEW, C. L., YEARLEY, J. H., SHINTAKU, I. P., TAYLOR, E. J., ROBERT, L., CHMIELOWSKI, B., SPASIC, M., HENRY, G., CIOBANU, V., WEST, A. N., CARMONA, M., KIVORK, C., SEJA, E., CHERRY, G., GUTIERREZ, A. J., GROGAN, T. R., MATEUS, C., TOMASIC, G., GLASPY, J. A., EMERSON, R. O., ROBINS, H., PIERCE, R. H., ELASHOFF, D. A., ROBERT, C. & RIBAS, A. 2014. PD-1 blockade induces responses by inhibiting adaptive immune resistance. *Nature*, 515, 568-71.
- UTZSCHNEIDER, D. T., CHARMOY, M., CHENNUPATI, V., POUSSE, L., FERREIRA, D. P., CALDERON-COPETE, S., DANILO, M., ALFEI, F., HOFMANN, M., WIELAND, D., PRADERVAND, S., THIMME, R., ZEHN, D. & HELD, W. 2016. T Cell Factor 1-Expressing Memory-like CD8(+) T Cells Sustain the Immune Response to Chronic Viral Infections. *Immunity*, 45, 415-27.
- UTZSCHNEIDER, D. T., GABRIEL, S. S., CHISANGA, D., GLOURY, R., GUBSER, P. M., VASANTHAKUMAR, A., SHI, W. & KALLIES, A. 2020. Early precursor

- T cells establish and propagate T cell exhaustion in chronic infection. *Nat Immunol*, 21, 1256-1266.
- WANG, D. Y., SALEM, J. E., COHEN, J. V., CHANDRA, S., MENZER, C., YE, F., ZHAO, S., DAS, S., BECKERMANN, K. E., HA, L., RATHMELL, W. K., ANCELL, K. K., BALKO, J. M., BOWMAN, C., DAVIS, E. J., CHISM, D. D., HORN, L., LONG, G. V., CARLINO, M. S., LEBRUN-VIGNES, B., EROGLU, Z., HASSEL, J. C., MENZIES, A. M., SOSMAN, J. A., SULLIVAN, R. J., MOSLEHI, J. J. & JOHNSON, D. B. 2018. Fatal Toxic Effects Associated With Immune Checkpoint Inhibitors: A Systematic Review and Meta-analysis. *JAMA Oncol*, 4, 1721-1728.
- WHELAN, S., OPHIR, E., KOTTURI, M. F., LEVY, O., GANGULY, S., LEUNG, L., VAKNIN, I., KUMAR, S., DASSA, L., HANSEN, K., BERNADOS, D., MURTER, B., SONI, A., TAUBE, J. M., FADER, A. N., WANG, T. L., SHIH, I. M., WHITE, M., PARDOLL, D. M. & LIANG, S. C. 2019. PVRIG and PVRL2 Are Induced in Cancer and Inhibit CD8(+) T-cell Function. *Cancer Immunol Res*, 7, 257-268.
- XU, F., SUNDERLAND, A., ZHOU, Y., SCHULICK, R. D., EDIL, B. H. & ZHU, Y. 2017. Blockade of CD112R and TIGIT signaling sensitizes human natural killer cell functions. *Cancer Immunol Immunother*, 66, 1367-1375.
- YARCHOAN, M., HOPKINS, A. & JAFFEE, E. M. 2017. Tumor Mutational Burden and Response Rate to PD-1 Inhibition. *N Engl J Med*, 377, 2500-2501.
- ZHOU, Z., XIE, X., WANG, X., ZHANG, X., LI, W., SUN, T., CAI, Y., WU, J., DANG, C. & ZHANG, H. 2021. Correlations Between Tumor Mutation Burden and Immunocyte Infiltration and Their Prognostic Value in Colon Cancer. *Front Genet*, 12, 623424.
- ZHU, Y., PANICCIA, A., SCHULICK, A. C., CHEN, W., KOENIG, M. R., BYERS, J. T., YAO, S., BEVERS, S. & EDIL, B. H. 2016. Identification of CD112R as a novel checkpoint for human T cells. *J Exp Med*, 213, 167-76.

11. Acknowledgments

Time flies and when I look back on my first day in Germany, it seems like yesterday. I would like to take this opportunity to express my sincere thanks and best wishes to all the professors, colleagues, and friends who have helped me during these two years.

First of all, my deepest gratitude goes to my supervisors, Prof. Sauter and Prof. Simon, for providing me with the opportunity to come from China to Germany to pursue my MD degree. I appreciate their guidance and quality control of my thesis.

Besides, I would like to sincerely thank Niclas walking me through the whole experiment and thesis. Thank you for his praise and encouragement when we made progress and for his tolerance and comfort when our experiments failed. His meticulous attitude towards scientific research and his pursuit of truth also made a profound impression on me and help me understand the true meaning and joy of scientific research. The rigorous attitude will be the cornerstone of my future research path.

Moreover, I would like to thank my colleagues, such as Tim, Elena, Hannah, Julia. I would like to thank them for their help in life and study. Thanks to Tim and Hannah for patiently teaching me basic knowledge and skills when I first joined the lab, and Elena for solving the difficulties that come with the German language: helping me with phone calls, emails, visa extensions, and frequent bus rides together. Thanks to Julia for solving many technical problems during the experiment and providing technical support for the experiment.

Last but not least, I would like to thank my parents. For more than 20 years, they have been supporting me both spiritually and materially.

12. Curriculum Vitae

Der Lebenslauf wurde aus datenschutzrechtlichen Gründen entfernt

13. Eidesstattliche Versicherung

Ich versichere ausdrücklich, dass ich die Arbeit selbständig und ohne fremde Hilfe verfasst, andere als die von mir angegebenen Quellen und Hilfsmittel nicht benutzt und die aus den benutzten Werken wörtlich oder inhaltlich entnommenen Stellen einzeln nach Ausgabe (Auflage und Jahr des Erscheinens), Band und Seite des benutzten Werkes kenntlich gemacht habe.

Ferner versichere ich, dass ich die Dissertation bisher nicht einem Fachvertreter an einer anderen Hochschule zur Überprüfung vorgelegt oder mich anderweitig um Zulassung zur Promotion beworben habe.

Ich erkläre mich einverstanden, dass meine Dissertation vom Dekanat der Medizinischen Fakultät mit einer gängigen Software zur Erkennung von Plagiaten überprüft werden kann.

Unterschrift: 